Linking mineralogy and spectroscopy of highly aqueously altered CM and CI carbonaceous chondrites in preparation for primitive asteroid sample return

The Meteoritical Society

Meteoritics & Planetary Science 1–25 (2019)
doi: 10.1111/maps.13411

Linking mineralogy and spectroscopy of highly aqueously altered CM and CI carbonaceous chondrites in preparation for primitive asteroid sample return

H. C. BATES[1,2*], A. J. KING[1,3], K. L. DONALDSON HANNA[2,4], N. E. BOWLES[2], and S. S. RUSSELL[1]

[1]Planetary Materials Group, Department of Earth Sciences, Natural History Museum, Cromwell Road, London SW7 5BD, UK
[2]Atmospheric, Oceanic and Planetary Physics, University of Oxford, Oxford OX1 3PU, UK
[3]School of Physical Sciences, The Open University, Milton Keynes MK7 6AA, UK
[4]Department of Physics, University of Central Florida, 4111 Libra Drive, Orlando, Florida 32816, USA
[*]Corresponding author. E-mail: h.bates@nhm.ac.uk

(Received 24 April 2019; revision accepted 01 October 2019)

Abstract–The highly hydrated, petrologic type 1 CM and CI carbonaceous chondrites likely derived from primitive, water-rich asteroids, two of which are the targets for JAXA's Hayabusa2 and NASA's OSIRIS-REx missions. We have collected visible and near-infrared (VNIR) and mid infrared (MIR) reflectance spectra from well-characterized CM1/2, CM1, and CI1 chondrites and identified trends related to their mineralogy and degree of secondary processing. The spectral slope between 0.65 and 1.05 μm decreases with increasing total phyllosilicate abundance and increasing magnetite abundance, both of which are associated with more extensive aqueous alteration. Furthermore, features at ~3 μm shift from centers near 2.80 μm in the intermediately altered CM1/2 chondrites to near 2.73 μm in the highly altered CM1 chondrites. The Christiansen features (CF) and the transparency features shift to shorter wavelengths as the phyllosilicate composition of the meteorites becomes more Mg-rich, which occurs as aqueous alteration proceeds. Spectra also show a feature near 6 μm, which is related to the presence of phyllosilicates, but is not a reliable parameter for estimating the degree of aqueous alteration. The observed trends can be used to estimate the surface mineralogy and the degree of aqueous alteration in remote observations of asteroids. For example, (1) Ceres has a sharp feature near 2.72 μm, which is similar in both position and shape to the same feature in the spectra of the highly altered CM1 MIL 05137, suggesting abundant Mg-rich phyllosilicates on the surface. Notably, both OSIRIS-REx and Hayabusa2 have onboard instruments which cover the VNIR and MIR wavelength ranges, so the results presented here will help in corroborating initial results from Bennu and Ryugu.

INTRODUCTION

The C-complex asteroids, which include the B-, C-, Cb-, Cg-, Cgh-, and Ch-types in the Bus-DeMeo classification scheme (DeMeo et al. 2009), are of interest because they are thought to be chemically primitive, volatile-rich, and can tell us about the evolution of water and organic compounds in the early solar system (e.g., Alexander et al. 2012). NASA's Dawn mission was the first to comprehensively investigate a C-type asteroid, orbiting (1) Ceres for just over 3 years (e.g., Russell and Raymond 2011). Currently, JAXA's Hayabusa2 is at the Cg-type asteroid (162173) Ryugu, and NASA's Origins, Spectral Interpretation, Resource Identification, Security, Regolith Explorer (OSIRIS-REx, Lauretta et al. 2017) is at the B-type asteroid (101955) Bennu. Both missions aim to collect and return samples from the surfaces of their target asteroids. The returned samples will have geological context (provided by the remote sensing instruments on the spacecraft) and will not be subject to any terrestrial contamination, providing an unprecedented opportunity to study the formation and

evolution of primitive solar system bodies (Tachibana et al. 2014; Lauretta et al. 2017).

Carbonaceous chondrite meteorites are hypothesized to be samples of C-complex asteroids (Greenberg and Chapman 1983; Tholen 1984), particularly the hydrated CM and CI carbonaceous chondrites, suggesting a history of aqueous alteration in the C-complex class (Vilas 1994; Burbine et al. 2002; Cloutis et al. 2011a; Licandro et al. 2012; Vernazza et al. 2016). Aqueous alteration occurred when accreted ices melted and the resulting fluids reacted with the original anhydrous mineralogy to form secondary minerals. In the CM chondrites, these include phyllosilicates, carbonates, oxides, and sulfides (Brearley 2006). Over 95% of CMs are classified as type 2 meteorites having suffered only partial alteration of the original anhydrous mineralogy; however, a small number (~25) are classified as petrologic type 1 (Zolensky et al. 1997). Aqueous alteration of CM chondrites is inferred to have occurred under water/rock ratios of 0.3–0.6 and at temperatures <100 °C (DuFresne and Anders 1962; Clayton and Mayeda 1984, 1999; Zolensky et al. 1989; Guo and Eiler 2007). The CI chondrites contain abundant phyllosilicates, as well as significant magnetite (~10 vol%), and minor sulfides and carbonates (Brearley 2006; King et al. 2015a). The CIs are all classified as petrologic type 1 meteorites and record aqueous alteration at high water/rock ratios of 1.1–1.2 and temperatures of ~150 °C (Tomeoka and Buseck 1988; Endress et al. 1996; Clayton and Mayeda 1999; Barrat et al. 2012; King et al. 2015a).

Associations between C-complex asteroids and the CM and CI chondrites have been made based on similarities in their visible and near-infrared (VNIR; 0.6–5 μm) and mid-infrared (MIR; 5–30 μm) spectra (e.g., Vilas et al. 1994; Burbine et al. 2002; Licandro et al. 2012; Takir et al. 2015). We can therefore use CM and CI chondrites to study the composition of asteroid surfaces, by linking trends in well-characterized mineralogy and alteration history to features in laboratory spectra, and then applying that knowledge to asteroid spectra. The VNIR spectral range in CM and CI chondrites shows absorption features at 0.7 and ~3 μm; however, using this range to uniquely identify mineralogy is challenging (e.g., Cloutis et al. 2011a, 2011b). Spectral slopes between ~0.6 and 2.4 μm have been linked to the phyllosilicate content of meteorites; McAdam et al. (2015) found a flattening of the VNIR spectral slope with increasing phyllosilicate content in CM and CI chondrites but noted that grain size, metal abundance, and terrestrial weathering might also contribute to variability. The 0.7 μm feature, hypothesized to be caused by charge transfer between Fe^{2+} and Fe^{3+} in phyllosilicates or oxides, is potentially diagnostic of hydration (Vilas and Gaffey 1989; Clark 1999), but is not always observed in CM chondrite spectra (Cloutis et al. 2011b). In remote asteroid observations, the 0.7–2.4 μm spectral shape and 0.7 μm band depth have been used to link CM chondrites to Ch- and Cgh-type asteroids, suggesting they are hydrated bodies (Vernazza et al. 2016). The 3 μm feature is caused by fundamental vibrations of water and hydroxyl groups (Gaffey et al. 1993), and the position, shape, and depth have been related to the mineralogy of CM and CI chondrites (Beck et al. 2010, 2014; Takir et al. 2013). Additionally, Takir et al. (2015) used this relationship to make some initial identifications of the surface mineralogy and extent of aqueous alteration of outer Main Belt, C-complex asteroids using remote observations collected at the NASA Infrared Telescope Facility (IRTF).

In contrast to the VNIR region, the MIR wavelength range contains a number of diagnostic features in CI and CM spectra (Salisbury 1993), so combining the two spectral ranges will provide more robust determinations of composition. Some silicate minerals have absorption features between 4 and 7 μm, which result from overtones and combinations of fundamental molecular vibrations. These can be prominent in fine powders and could be useful for identifying mineralogy (Salisbury and Walter 1989; Salisbury et al. 1991). The Christiansen feature (CF), between 7.5 and 9 μm, is unique to each mineral, so in complex materials such as meteorites it is often found to be a combination of the CFs of each component present (Salisbury et al. 1991). While McAdam et al. (2015) reported no correlation between the position of the CF and mineralogy of the CM and CI chondrites, its shape was found to become sharper with increasing phyllosilicate abundances and higher degrees of aqueous alteration. The transparency features (TFs), between 11 and 13 μm, are caused by volume scattering in fine particulate, optically thin materials (Salisbury 1993; Cooper 2002). Due to the relationship of the TF to the fundamental vibration bands, this region is expected to be diagnostic of composition in fine particulate samples (Salisbury and Walter 1989). McAdam et al. (2015) investigated a number of CM and CI chondrites with grain size <35 μm and found a correlation between features in the TF region and phyllosilicate abundance, with features shifting to shorter wavelengths with increasing phyllosilicate abundance.

Most spectral studies have focused on the partially altered CM2 meteorites (e.g., Salisbury et al. 1991), and if petrologic type 1 chondrites are included, they are treated more as endmembers of the petrologic sequence (Cloutis et al. 2011b; Takir et al. 2013; McAdam et al. 2015). However, preliminary results from Hayabusa2 suggest that the surface of asteroid Ryugu resembles thermally metamorphosed CM/CI-like material (Kitazato et al.

2019), and preliminary survey observations from OSIRIS-REx indicate that Bennu's surface may consist of highly altered CM1 and/or CI1-like materials (Hamilton et al. 2019). In addition, McSween et al. (2017) concluded that Ceres has experienced extensive aqueous alteration similar to that recorded in the CM1 and CI1 chondrites. Here, we have collected VNIR and MIR reflectance spectra from highly altered CM1/2, CM1, and CI1 chondrites, using exactly the same meteorite samples for which modal mineralogy was determined by King et al. (2017) and King et al. (2015a). Our aim was to directly relate spectral trends to known composition and alteration history so that observed spectral properties could be related to asteroid surface mineralogy and processing. This enables further exploration of the relationship of primitive bodies to highly aqueously altered CM and CI chondrites.

EXPERIMENTAL

Samples

Our sample suite consisted of two CI chondrites: Orgueil and Ivuna (Org-1 and Ivu-1 in King et al. 2015a; (1) five CM1/2 chondrites: MacKay Glacier (MCY) 05231, LaPaz Icefield (LAP) 031214, Miller Range (MIL) 090288, LAP 031166, and Northwest Africa (NWA) 8534, and six CM1 chondrites: Grosvenor Mountains (GRO) 95645, NWA 4765, LAP 02277, MIL 05137, MIL 07689, and Moapa Valley. For comparison, we also measured the CM2 chondrite Murchison. The samples were the same powders (particle sizes <35 μm) for which King et al. (2015a) and King et al. (2017) determined bulk modal mineral abundances using X-ray diffraction, and their results are in Table 1 (except for Murchison, where the abundances are taken from Howard et al. 2015). The CM chondrites contain abundant phyllosilicates (71–91 vol%), olivine (4–20 vol%), enstatite (1–8 vol%), magnetite (1–3 vol%), Fe-sulfide (<4 vol%), and calcite (<2 vol%), and several also contain gypsum (<1–3 vol%). The CI chondrites contain phyllosilicates (~84 vol%), magnetite (~8 vol%), Fe-sulfide (~6 vol%), and dolomite (<2 vol%). Orgueil also contains ferrihydrite (~2 vol%) and gypsum (1 vol%), which were not detected in Ivuna.

Comparisons to endmember standards are useful for identifying features and trends, although they cannot be used to determine exact mineralogy. Therefore, we also obtained spectra for mineral endmembers including the Mg-rich serpentines lizardite and antigorite (from the Natural History Museum [NHM], London collection, BM no. 66586), the Fe-rich serpentine cronstedtite (BM no. 52294; from herein Fe-cronstedtite), and saponite (BM no. 1938, 1255). However, we note that phyllosilicates in CM and CI chondrites are complex and not the same as our terrestrial endmember standards (e.g., Howard et al. 2009). For example, the serpentine family forms a solid solution between Fe and Mg endmembers, but in CM chondrites, these compositions are not reached (Tomeoka and Buseck 1985; Lauretta et al. 2000). Additionally, differences in crystallinity between the terrestrial standards and those phyllosilicates in CM and CI chondrites could also play a role in spectral variations.

Reflectance Spectroscopy

Visible and near-infrared (0.8–5 μm) and MIR (5–30 μm) reflectance spectra were collected for the CM1/2, CM1, and CI1 chondrites and mineral endmembers. Infrared reflectance spectra were obtained using a Bruker VERTEX 70v Fourier Transform Infrared spectrometer in diffuse reflectance geometry with a Specac Selector diffuse reflectance accessory at the Planetary Spectroscopy Facility (PSF) at the University of Oxford. All observations were obtained under vacuum (~2 hPa) at a spectral resolution of 4 cm^{-1}, and the resulting spectra were the average of 250 scans. A wide range mid- to far-IR (MIR-FIR) beam splitter and a room temperature deuterated L-alanine doped triglycine sulfate (RT-DLaTGS) detector were used to measure the reflectance between ~1.7 and 50 μm (6000–200 cm^{-1}). For these wavelength ranges, samples were measured before and after being heated at ~150 °C for 2.5 h, in order to remove the effects of terrestrial adsorbed water on the resulting spectra (e.g., Takir et al. 2013; Beck et al. 2014). A VIS/Q beam splitter and a combination of a Si-diode detector and an Indium Gallium Arsenide (InGaAs) detector were used to measure reflectance between 0.8 and 1.7 μm (12,500–6000 cm^{-1}). These measurements were performed only on the unheated samples as this spectral region is unaffected by adsorbed terrestrial water (Gaffey et al. 1993; McAdam et al. 2015). To remove instrument effects, each meteorite spectrum was divided by the spectrum of a Spectralon (a diffusely reflecting fluoropolymer) target between 0.8 and 1.7 μm, and by the spectrum of a diffuse gold calibration target between 1.7 and 50 μm, which were measured using the same experimental parameters and under the same conditions as the samples.

For analysis of the spectra, several diagnostic parameters were calculated, including spectral slope in the VNIR; the position and area of the feature at ~3 μm; and the positions of the 6 μm feature, the CF and the TF. For calculation of the VNIR spectral slope, data were normalized to unity at 0.8 μm and the slope was calculated as the reflectance at 1.65 μm divided by the reflectance at 1.05 μm. The point at which reflectance was taken was varied between 1.6–1.7 μm

Table 1. Bulk mineralogy of the CM1/2, CM1, and CI1 chondrite powders, as determined by King et al. (2015a) and King et al. (2017). Abundances for the CM2 Murchison are from Howard et al. (2015), although the same powder was not used in this study. The PSF (phyllosilicate fraction = total phyllosilicate abundance/total anhydrous silicate + total phyllosilicate abundance) is used to assign a petrologic type to each sample in the Howard et al. (2015a) classification scheme.

Sample	Classification	PSF petrologic type	Olivine (vol%)	Enstatite (vol%)	Magnetite (vol%)	Sulfide (vol%)	Carbonates (vol%)	Gypsum (vol%)	Ferrihydrite (vol%)	Fe-cronstedtite (vol%)	Mg-serpentine (vol%)	Total phyllosilicate (vol%)
Murchison	CM2	1.5	15.1	8.3	1.1	1.8	1.2	–	–	50.3	22.2	72.5
LAP031214	CM1/2*	1.5	18.2	5.9	2.3	1.1	1.0	0.3	–	30.8	40.4	71.2
MCY05231	CM1/2*	1.5	19.6	3.4	1.6	1.3	1.0	–	–	36.9	36.2	73.1
MIL090288	CM1/2	1.2	3.8	3.0	2.3	2.3	0.9	3.3	–	18.2	66.2	84.4
LAP031166	CM1/2	1.2	5.0	1.5	2.0	1.4	0.9	2.4	–	21.5	65.3	86.8
NWA8534	CM1/2	1.2	5.1	1.5	2.9	1.7	0.7	–	–	20.0	68.1	88.1
GRO95645	CM1	1.2	8.0	-	3.2	3.3	1.2	–	–	31.9	52.4	84.3
NWA4765	CM1	1.2	3.6	2.3	3.3	2.4	0.9	–	–	15.9	71.6	87.5
LAP02277	CM1	1.2	5.3	–	1.9	2.2	1.7	–	–	20.6	68.3	88.9
Moapa Valley	CM1	1.1	4.1	–	3.1	4.4	0.9	–	–	20.4	67.1	87.5
MIL05137	CM1	1.1	3.6	–	2.7	2.0	0.9	1.7	–	17.9	71.2	89.1
MIL07689	CM1	1.1	3.8	–	3.1	0.1	0.4	1.7	–	20.6	70.3	90.1
Orgueil (Org-1)	CI1	1.1	–	–	7.0	6.0	–	1.0	2.0	–	–	84.0
Ivuna (Ivu-1)	CI1	1.1	–	–	8.0	6.0	2.0	–	–	–	–	84.0

*These samples were inferred by King et al. (2017) to be CM2 chondrites rather than their official classification as CM1/2 chondrites.

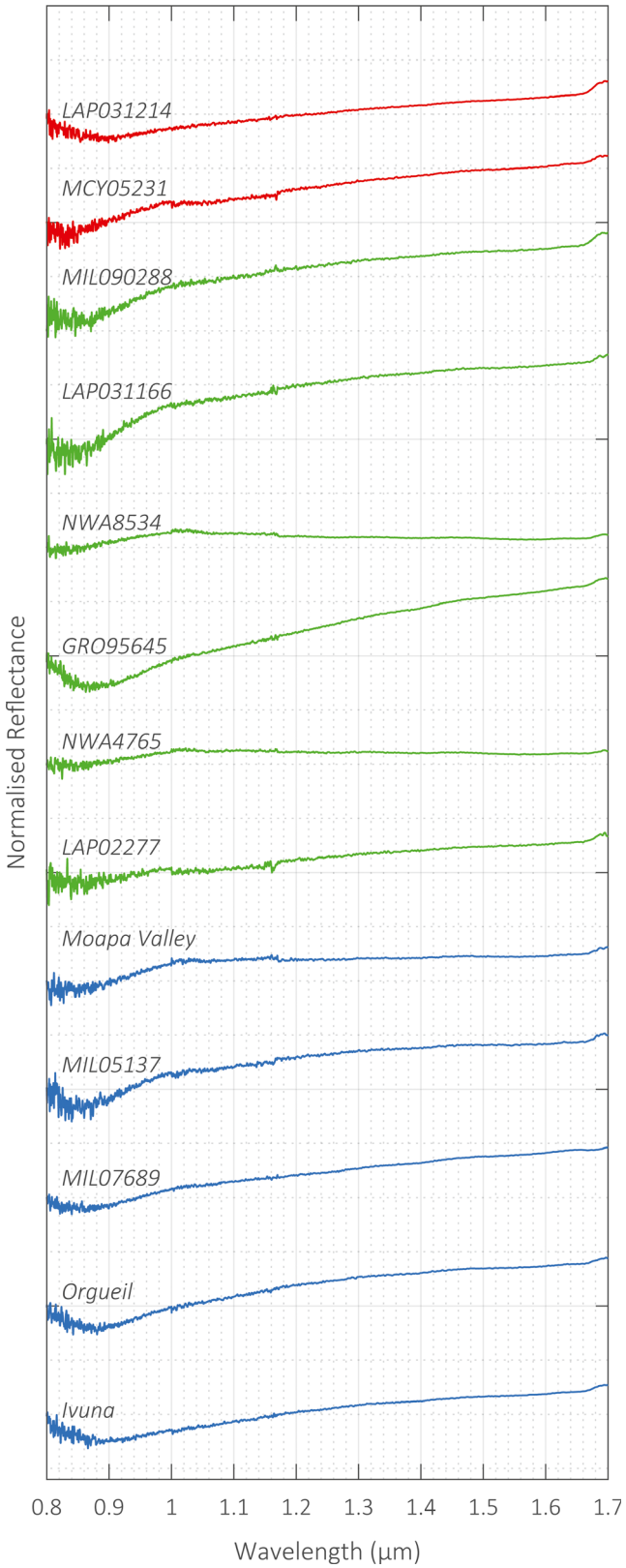

Fig. 1. VNIR spectra of CM1/2, CM1, and CI1 chondrites. Colors are representative of different PSF petrologic types, with blue—1.1, green—1.2, and red—1.5. For details of PSF, see Table 1. Spectra are normalized at 0.8 μm and offset for clarity. The spectra are featureless but do exhibit an increase in reflectance with increasing wavelength (red slope).

and 1–1.1 μm and an average calculated. These points were chosen to ensure the maximum range without noise or artifacts was used for calculations. The error in the slope was calculated as one standard deviation representing variation from the average.

For feature position and area, the region investigated was isolated and smoothed with a moving average of 10–15, enough to remove noise, but not to the point that the spectral shape of the feature was affected. A wavelength grid was generated across the region with an increment of 2×10^{-4} μm, and a third-order polynomial was fit across the center of the feature, which was used to calculate feature position and area (Donaldson Hanna et al. 2012). Feature position was established to be the point of minimum or maximum reflectance. Feature area was calculated on normalized data by fitting a continuum as a straight line between two points on either side of the feature and calculating the area between the continuum and the continuum removed spectra. The uncertainties are presented as one standard deviation, representing variability from the average of calculated parameters.

RESULTS

Visible and Near-Infrared

Figure 1 shows the spectra between 0.8 and 1.7 μm for CM1/2, CM1, and CI1 chondrites. Figure 2A shows the same wavelength range for the phyllosilicate standards. The meteorite spectra are mostly featureless and generally show a red slope (increasing reflectance with increasing wavelength). NWA 8534, NWA 4765, and Moapa Valley show the flattest spectra, with slopes of 0.96, 0.98, and 1.08, compared to the steeper slopes (1.23–1.61) of the other CMs. Orgueil and Ivuna show spectral slopes of 1.35 and 1.37, respectively (Table 2).

The red slopes are partly influenced by particle size (Cloutis et al. 2011b); however, our meteorite samples (and standards) were all prepared in the same way and have similar particle sizes of <35 μm (e.g., King et al. 2015a; King et al. 2017), so any variation in slope within the suite should be a function of mineralogy. Based on this assumption, the spectral red slope in most of the meteorite samples is likely due to their high phyllosilicate abundances (71–90 vol%), as the representative mineral endmembers also show red spectral slopes (Fig. 2A).

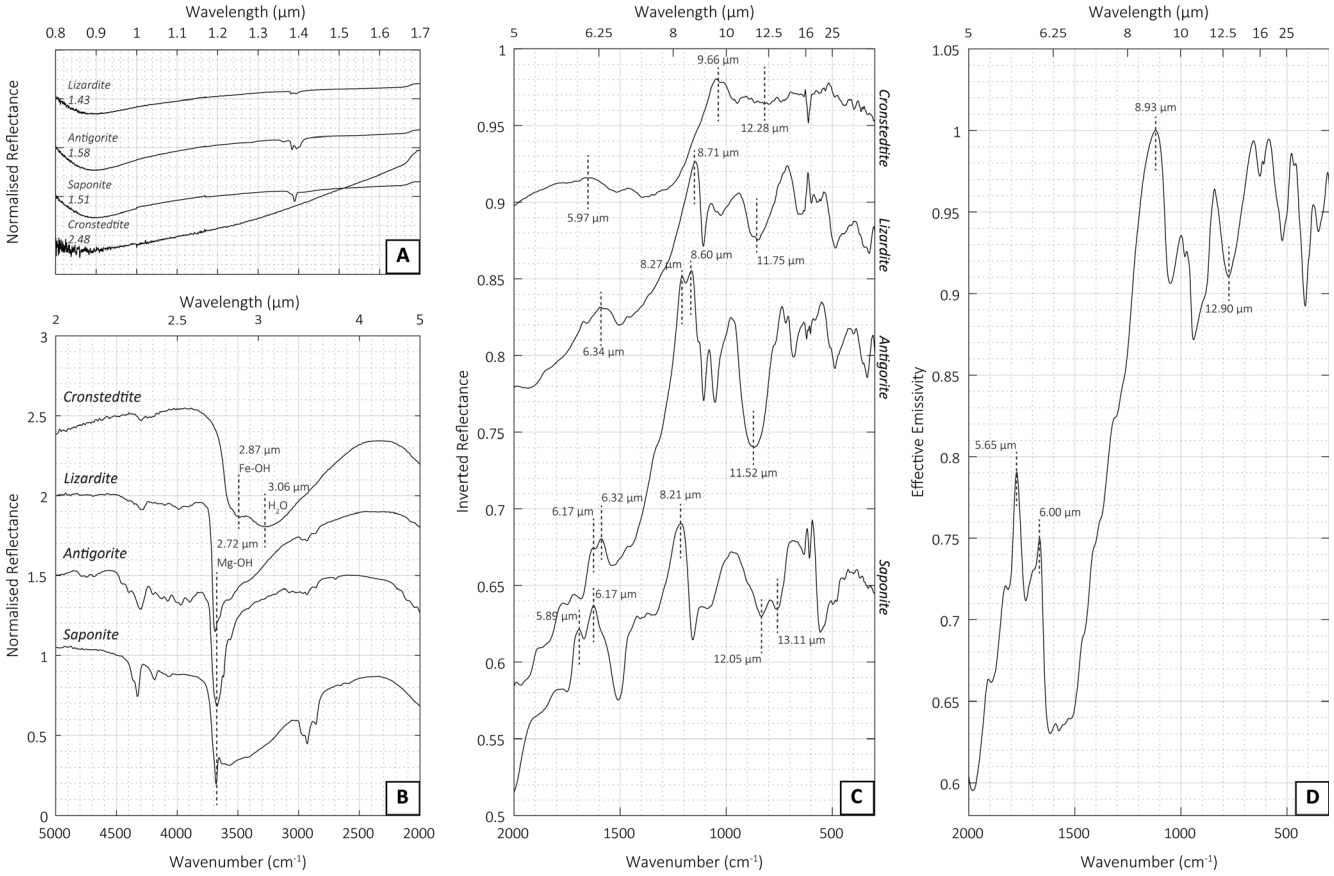

Fig. 2. A) VNIR spectra for the serpentine minerals cronstedtite, lizardite, and antigorite and the smectite mineral saponite. Spectra are normalized to unity at 0.8 μm and offset for clarity. Ratios are calculated as the reflectance at 1.65 μm divided by the reflectance at 1.05 μm are included on the figure. B) The 3 μm feature for the serpentine phyllosilicates cronstedtite, lizardite, and antigorite and the smectite phyllosilicate saponite. Spectra are normalized to unity at 2.3 μm and offset for clarity. Features of interest are marked on the figure. C) MIR spectra for the serpentine phyllosilicates cronstedtite, lizardite, and antigorite and the smectite phyllosilicate saponite. Spectra are inverted and offset for clarity. Features of interest are marked on the figure. D) The emissivity spectrum of San Carlos Olivine in the MIR wavelength ranges. Features of interest are marked on the figure.

The 3 μm region for the phyllosilicate standards is shown in Fig. 2B. The spectra of our Mg-rich serpentine standards (lizardite and antigorite) show sharp 3 μm features with band centers at 2.72 μm, caused by Mg-OH (Fig. 2B). The Fe-cronstedtite spectrum shows a more rounded feature, with two minima that can be identified at 2.87 and 3.06 μm (Fig. 2B). The 3.06 μm feature in our Fe-cronstedtite spectral measurement was also observed by Takir et al. (2013) in an unheated Fe-cronstedtite spectrum. We assume that this feature is due to terrestrial contamination, for example, Fe-(oxy)hydroxides, which are known to have features near 3.06 μm (Bishop et al. 1993; Pommerol et al. 2009). Overall, in the 3 μm region, the spectra of our phyllosilicate standards match well with previous spectral measurements of similar standards (e.g., Salisbury et al. 1991; Takir et al. 2013).

All the meteorite spectra show a large, asymmetric absorption feature between ~2.70 and 4.00 μm (Fig. 3; Table 2), suggesting they all contain mineral phases which have bound OH or H_2O. As the samples were heated prior to measurement, and spectra were collected under vacuum, we attribute these features to the presence of hydrated mineral phases rather than adsorbed terrestrial water. There may still be some water trapped in high-energy sites which may contribute to the 3 μm feature (Beck et al. 2010); however, thermogravimetric analysis (TGA) shows most of the molecular and mesopore water is removed on heating up to 150–200 °C (Garenne et al. 2014). Murchison (CM2), MCY 05231, and LAP 031214 spectra show rounded features, with centers between 2.79 and 2.82 μm (Fig. 3A), whereas the other CM1/2 and CM1 chondrite spectra have much sharper features, with centers between 2.73 and 2.74 μm (Figs. 3B and 3C).

Table 2. The parameters for the VNIR and MIR features described in the text.

		VNIR slope	3 μm feature (μm)	3 μm feature area	6 μm feature (μm)	CF center (μm)	TF center (μm)
CM	Murchison	–	2.82 ± 0.01	0.18 ± 0.02	6.14 ± 0.01	9.12 ± 0.04	12.51 ± 0.07
	LAP031214	1.35 ± 0.08	2.78 ± 0.01	0.15 ± 0.03	6.13 ± 0.01[a]	8.98 ± 0.02	11.82 ± 0.06
	MCY05231	1.31 ± 0.04	2.81 ± 0.01	0.14 ± 0.02	6.15 ± 0.01	9.10 ± 0.03	12.31 ± 0.09
	MIL090288	1.24 ± 0.05	2.73 ± 0.01	0.09 ± 0.04	6.14 ± 0.01	9.01 ± 0.05	11.73 ± 0.07
	LAP031166	1.28 ± 0.04	2.74 ± 0.01	0.08 ± 0.03	6.10 ± 0.01	8.88 ± 0.04	11.36 ± 0.10
	NWA8534	0.96 ± 0.01	2.74 ± 0.01	0.10 ± 0.03	6.26 ± 0.01	9.05 ± 0.06	11.74 ± 0.06
	GRO95645	1.61 ± 0.10	2.73 ± 0.01	0.26 ± 0.06	6.15 ± 0.01[a]	8.75 ± 0.03	11.53 ± 0.10
	NWA4765	0.98 ± 0.01	2.74 ± 0.01	0.06 ± 0.03	6.18 ± 0.02	8.88 ± 0.05	11.53 ± 0.10
	LAP02277	1.25 ± 0.03	2.73 ± 0.01	0.06 ± 0.04	6.19 ± 0.03	8.96 ± 0.05	11.67 ± 0.08
	Moapa Valley	1.08 ± 0.03	2.74 ± 0.01	0.05 ± 0.03	6.24 ± 0.05	9.06 ± 0.06	11.95 ± 0.09
	MIL05137	1.23 ± 0.04	2.74 ± 0.01	0.09 ± 0.04	6.13 ± 0.01	9.01 ± 0.05	11.69 ± 0.07
	MIL07689	1.30 ± 0.04	2.74 ± 0.01	0.23 ± 0.05	6.17 ± 0.01[a]	8.85 ± 0.03	11.62 ± 0.08
	Orgueil (Org-1)	1.35 ± 0.06	2.72 ± 0.01[b]	0.23 ± 0.01	6.12 ± 0.02[a]	8.79 ± 0.03	11.58 ± 0.06
CI	Ivuna (Ivu-1)	1.37 ± 0.06	2.72 ± 0.01[b]	0.22 ± 0.01	6.10 ± 0.03[a]	8.80 ± 0.02	11.56 ± 0.08

[a]These 6 μm features also have a shoulder at ~5.80 μm.
[b]Orgueil and Ivuna additionally show a broad feature at 2.98 ± 0.01 μm and 3.01 ± 0.03 μm, respectively.

Some sample spectra also show a minor feature near 3.40 μm, which in previous studies has been attributed to organics (Takir et al. 2013). Band areas in this region are between 0.05 and 0.18 μm^{-1}, except for MIL 07689 and GRO 95645, which have larger band areas of 0.23 and 0.26 μm^{-1}, respectively (Table 2). The CI1 chondrites Orgueil and Ivuna spectra show a sharp feature at 2.72 μm, alongside a broader feature centered at 2.98 and 3.01 μm, respectively (Fig. 4). The band area is 0.23 μm^{-1} for Orgueil and 0.22 μm^{-1} for Ivuna, and spectra for both also show an organic feature near 3.40 μm. The shape and position of these features in our meteorite spectra are similar to the features in the spectra of the phyllosilicate standards we measured, and are consistent with previous spectral measurements in other carbonaceous chondrites (e.g., Takir et al. 2013).

Mid Infrared

Figures 5 and 6 show the MIR spectra of the CM1/2, CM1, and CI1 chondrites. Also shown in Fig. 5 is the MIR spectrum for the less altered CM2 chondrite Murchison. Figure 2C shows the MIR spectra for the phyllosilicate standards and Fig. 2D shows the emissivity spectrum for San Carlos Olivine. In the 5–7 μm range, all the CM chondrite spectra show a feature between 6.10 and 6.26 μm. In addition, the LAP 031214, GRO 95645, and MIL 07689 spectra also show a slight shoulder at ~5.8 μm. The CI1 chondrite spectra show a feature in this region, at 6.12 and 6.10 μm, respectively, with a shoulder at ~5.8 μm (Fig. 6). Between 5 and 7 μm, Si-O, OH-, and H_2O all have vibrational absorption features, and as such all standard spectra show features in this region (Fig. 2C). As with the 3 μm feature, there is chance that some water remains in high-energy sites and could be contributing to these features (Beck et al. 2010). Additionally, some organics are known to have features in this region, for example, carbonyl near 5.9 μm and aromatic carbon near 6.25 μm (Battandier et al. 2018). Due to the presence of features between 5 and 7 μm in the silicate standards, however, and as our samples are heated prior to measurement, and spectra were collected under vacuum, we assume that these spectral features are related to mineralogy rather than adsorbed terrestrial water. Due to the high abundance of phyllosilicates in CM and CI chondrites, we believe the features in this region are more likely associated with hydrated mineralogy than anhydrous silicate minerals. This is consistent with the spectra, as the positions of the 6 μm features plot within the phyllosilicate range, and the vibrational features in olivine are observed at shorter wavelengths at 5.65 and 6.00 μm.

All the meteorite spectra show a CF between 8.75 and 9.12 μm (Figs. 5 and 6). The Murchison and MCY 05231 spectra show broad features, at 9.12 and 9.10 μm. The remaining CM spectra show sharper features at shorter wavelengths, between 8.75 and 9.06 μm. The CI chondrite spectra show broad features centered at 8.87 and 8.94 μm. Between 11 and 13 μm is a region of optical transparency in fine-grained material, resulting in a TF, and all our samples show a reflectance maximum (emissivity minimum) in this region. The Murchison and MCY 05231 spectra have TFs at slightly longer wavelengths than the other CMs at 12.51 and 12.31 μm, respectively. The remaining CM spectra show a spread of TFs between 11.36 and 11.95 μm. The CI spectra have TFs at 11.50 and 11.73 μm.

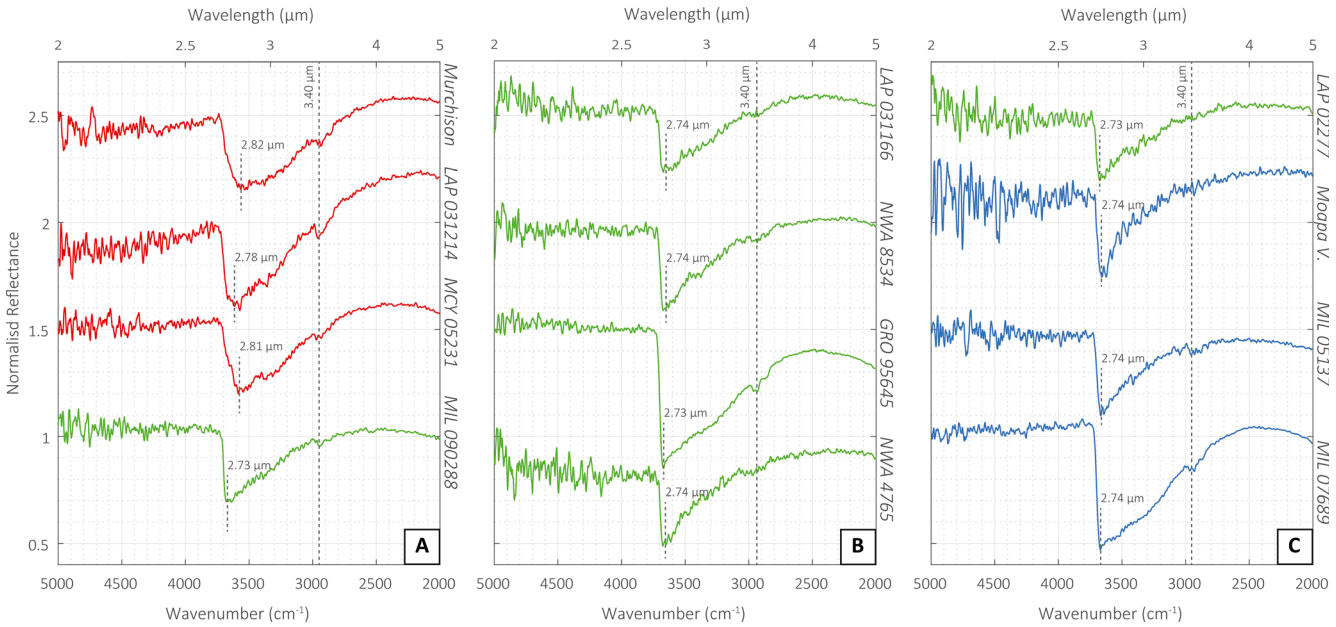

Fig. 3. The 3 μm feature for (A) Murchison, LAP 031214, MCY 05231, and MIL 090288; (B) LAP 031166, NWA 8534, GRO 95645, and NWA 4765; and (C) LAP 02277, Moapa Valley, MIL 05137, and MIL 07689. Red spectra are PSF petrologic type 1.5, green 1.2, and blue 1.1. Spectra are normalized to unity at 2.3 μm and offset for clarity. The features are characterized by a center between 2.73 and 2.82 μm, the location of which depends on the phyllosilicate composition. Some samples also show a minor feature at 3.40 μm attributed to organics.

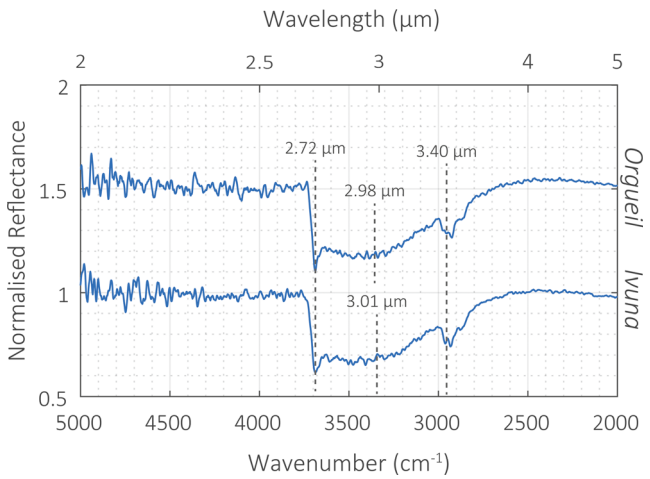

Fig. 4. The 3 μm feature for the CI chondrites Orgueil and Ivuna. The blue spectra reflect the PSF petrologic type 1.1. Spectra are normalized to unity at 2.3 μm and offset for clarity. There are three components to the 3 μm feature in the CIs: at 2.72 μm due to Mg-OH, at ~3.00 μm due to bound H_2O, and at 3.40 μm due to organics.

The positions of the CFs and TFs are consistent with the positions of the same features in the spectra of our mineral standards (Fig. 2), and are consistent with previous observations of the CF and TF in CM and CI chondrite spectra (e.g., McAdam et al. 2015). There does, however, appear to be a change in both shape and position of the CF and in position of the TF as aqueous alteration proceeds.

DISCUSSION

Visible and Near-IR Spectral Relationships to Mineralogy

VNIR Slope

Cloutis et al. (2011a, 2011b) showed that the spectral slope of CM and CI chondrites in the VNIR region is highly variable, ranging from red to blue (decreasing reflectance with increasing wavelength), and does not correlate with phyllosilicate composition. They also showed the same meteorite could show large differences in slopes between different subsamples. Opaque phases (e.g., complex organics, iron sulfide, magnetite) are expected to cause no change, or only modest reddening, in the VNIR slope of CM chondrites due to their low abundances (<5 vol%). In contrast, CI chondrites contain abundant magnetite (~10 vol%), which can cause a decrease in absorption band depths and overall reflectance (Cloutis et al. 2011a). The VNIR spectral slope of both CMs and CIs has also been found to be affected by physical properties such as particle size, with finer particle sizes, like the ones investigated in this study (<35 μm), generally resulting in redder slopes (Cloutis

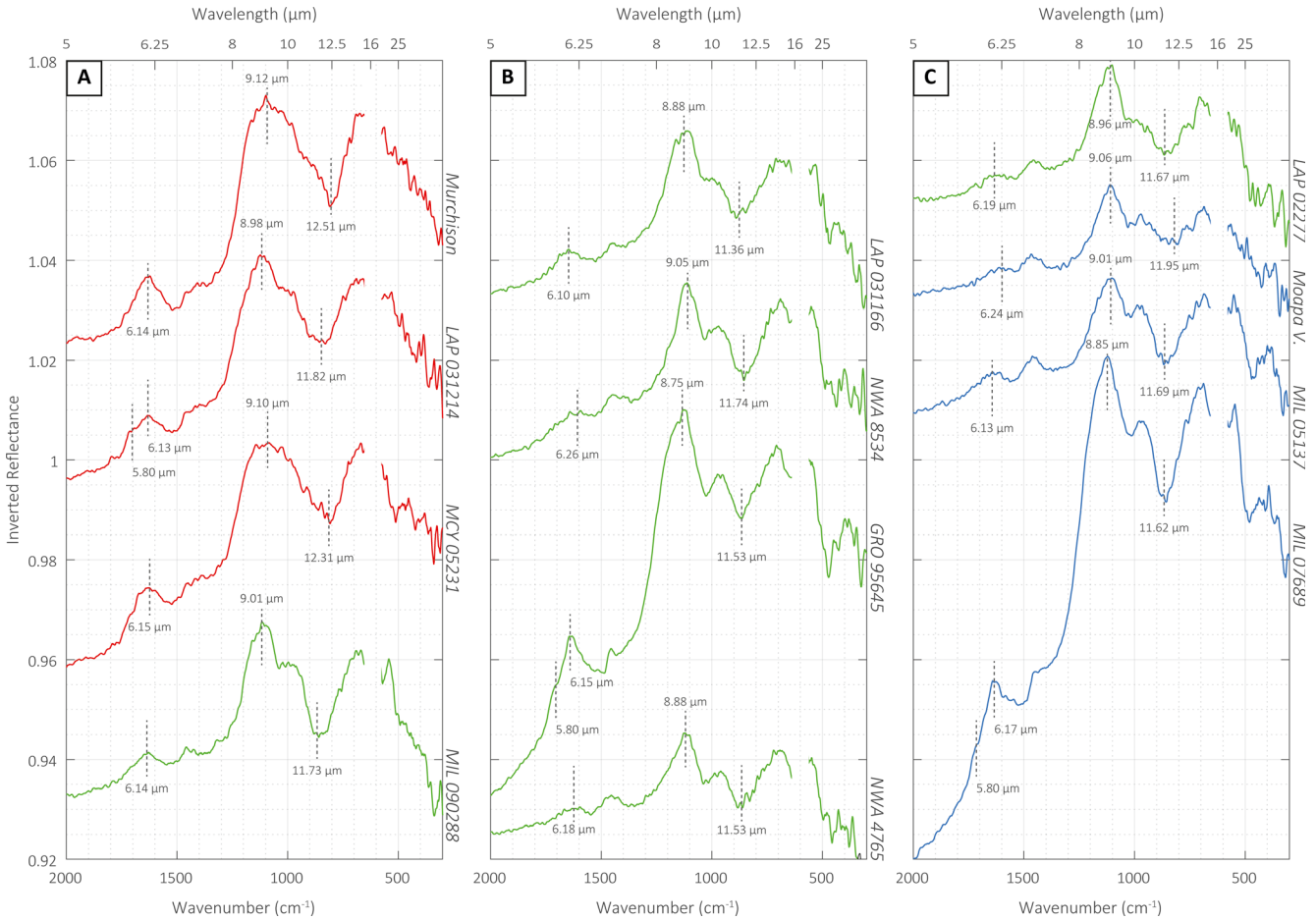

Fig. 5. MIR spectra for (A) Murchison, LAP 031214, MCY 05231, and MIL 090288; (B) LAP 031166, NWA 8534, GRO 95645, and NWA 4765; and (C) LAP 02277, Moapa Valley, MIL 05137, and MIL 07689. Red spectra are PSF petrologic type 1.5, green 1.2, and blue 1.1. Spectra are inverted and offset for clarity. All spectra show a feature near 6 μm due to combination and overtone vibrations of phyllosilicates, a Christiansen feature (CF) related to the optical constants of the constituent mineralogy, and a transparency feature (TF) in a region of optical transparency in fine-grained samples. These features are highlighted. The gap in the spectra is a region of low signal-to-noise due to the beamsplitter.

et al. 2011a, 2011b). McAdam et al. (2015) investigated a suite of CM chondrites ranging from petrologic type 2 to more aqueously altered type 1s, plus a single CI1 chondrite (Orgueil), and did find a relationship between spectral slope (0.56–2.4 μm) and mineralogy. They reported that the spectral slope becomes bluer and approached unity with increasing phyllosilicate abundance. Despite this trend, they suggested that NIR spectral slope is not a reliable metric for distinguishing composition due to the influence of other properties such as particle size, terrestrial weathering, and viewing geometry (McAdam et al. 2015).

The CM chondrite spectra with the reddest slope in this study are GRO 95645, with a slope of 1.61. This meteorite appears to have experienced significant terrestrial weathering, with a grade of B/Ce indicating the presence of visible evaporites and rusts (Grossman 1998). The CM1 chondrite MIL 07689 also has a high weathering grade of C (Ruzicka et al. 2015), and while it does not have the reddest spectral slope in the suite, its slope of 1.30 is higher than expected (see discussion below). Additionally, King et al. (2018) reported that the bulk oxygen isotopic compositions of GRO 95645 and MIL 07689 have clearly been influenced by Antarctic water. To test this further we analyzed GRO 95645 and MIL 07689 using TGA (for further details, see supporting information), which is a useful technique for identifying the presence and nature of hydrated phases. Previous analyses of CM chondrites using TGA have shown that common terrestrial weathering products (e.g., ferrihydrite and other Fe-(oxy)hydroxides) dehydrate and subsequently lose mass when heated to temperatures of

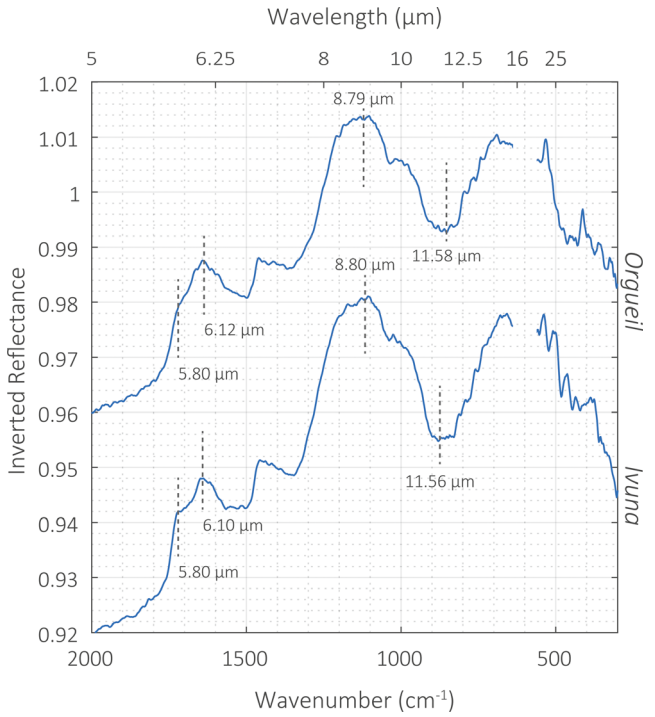

Fig. 6. MIR spectra for CI1 chondrites. The blue spectra reflect the PSF petrologic type 1.1. Spectra are inverted and offset for clarity. Both spectra show similar features to the CMs; near 6 μm, a Christiansen feature (CF) and a transparency feature (TF). These features are highlighted. The gap in the spectra is a region of low signal-to-noise due to the beamsplitter.

200–300 °C (Garenne et al. 2014). GRO 95645 and MIL 07689 both show a major mass loss event at ~225 °C (Fig. S1 in supporting information), which is consistent with the dehydration of ferrihydrite (Garenne et al. 2014; King et al. 2015b), and is not seen for the other CM1/2 and CM1 chondrites. This observation confirms that GRO 95645 and MIL 07689 are the most weathered meteorites analyzed in this study and contain a significant abundance of hydrated minerals formed by terrestrial weathering processes.

Cloutis et al. (2011b) showed that terrestrial weathering and the formation of rusts can make the spectral slopes of meteorites redder. For example, they attributed the strong red spectral slope (between 0.8 and 2.3 μm) of the highly weathered (grade Ce) Antarctic CM2 meteorite LEW 88001 to the presence of terrestrial Fe-(oxy)hydroxides. These phases have strong red slopes in the VNIR wavelength ranges. Similarly, we suggest that the red spectral slopes of GRO 95645 and MIL 07689 are the result of terrestrial weathering during the meteorites' residence in Antarctica. We note that all the CM chondrites in this study (except Murchison) are finds and likely experienced some terrestrial weathering. However, the absence of a dehydration event at ~225 °C in the TGA indicates that weathering was less severe for the other CM chondrites, making the spectral slope more reliable for identifying mineralogy associated with parent body alteration.

Phyllosilicates are the main minerals in CM and CI chondrites, and in general, their abundance increases with aqueous alteration (Howard et al. 2009, 2011). We find a weak trend (R^2 value of 0.27) between phyllosilicate abundance and spectral slope (Fig. 7A), with decreasing spectral slope as total phyllosilicate abundance increases (note that this trend does not include GRO 95645 and MIL 07689 as these spectra have redder slopes than expected for their phyllosilicate content due to terrestrial weathering). This relationship was also observed by McAdam et al. (2015), but is in contrast to observations by Cloutis et al. (2011a, 2011b), although in the case of the latter, only one CM1/2 was included in the study. Magnetite abundance has also been found to increase with aqueous alteration, and Cloutis et al. (2011a) showed that the addition of as little as 5 vol% magnetite to phyllosilicates causes the spectral slope to become bluer. We find VNIR spectral slope does decrease with increasing magnetite content in the CM1/2 and CM1 chondrites (excluding GRO 95645 and MIL 07689 and the CI chondrites; Fig. 7B), and this correlation is stronger (R^2 value of 0.68) than the relationship between spectral slope and total phyllosilicate abundance. Thus, we can conclude that magnetite is a more important control on VNIR spectral slope in the CM chondrites.

The spectra of the CI chondrites Orgueil and Ivuna show redder spectral slopes (1.35 and 1.37, respectively) than most of the CMs (Fig. 1). This is consistent with the observations of McAdam et al. (2015), who found that their Orgueil spectra had a redder slope than the most altered CM chondrites they investigated. Values of slope >1.3 are approximately what we would expect if phyllosilicate abundance was the main control on spectral slope (Fig. 7A). However, we can see in Fig. 7B the importance of magnetite content in the meteorites and CI chondrites have high magnetite abundances (~8 vol%), which the spectral slope does not seem to reflect. One explanation is that the spectral slopes are reflecting the phyllosilicate content of the CIs and are not affected by the magnetite abundances: CI chondrites are composed of intergrown serpentine and saponite and the spectra of our phyllosilicate standards also show strong red slopes (Fig. 2A). Alternatively, the Fe-(oxy)hydroxide ferrihydrite might be affecting slope. Ferrihydrite is a red-sloped material, and is found in Orgueil (King et al. 2015a). However, the similarity between the spectral slope in Ivuna and Orgueil suggests this is not the case, as ferrihydrite was not detected in

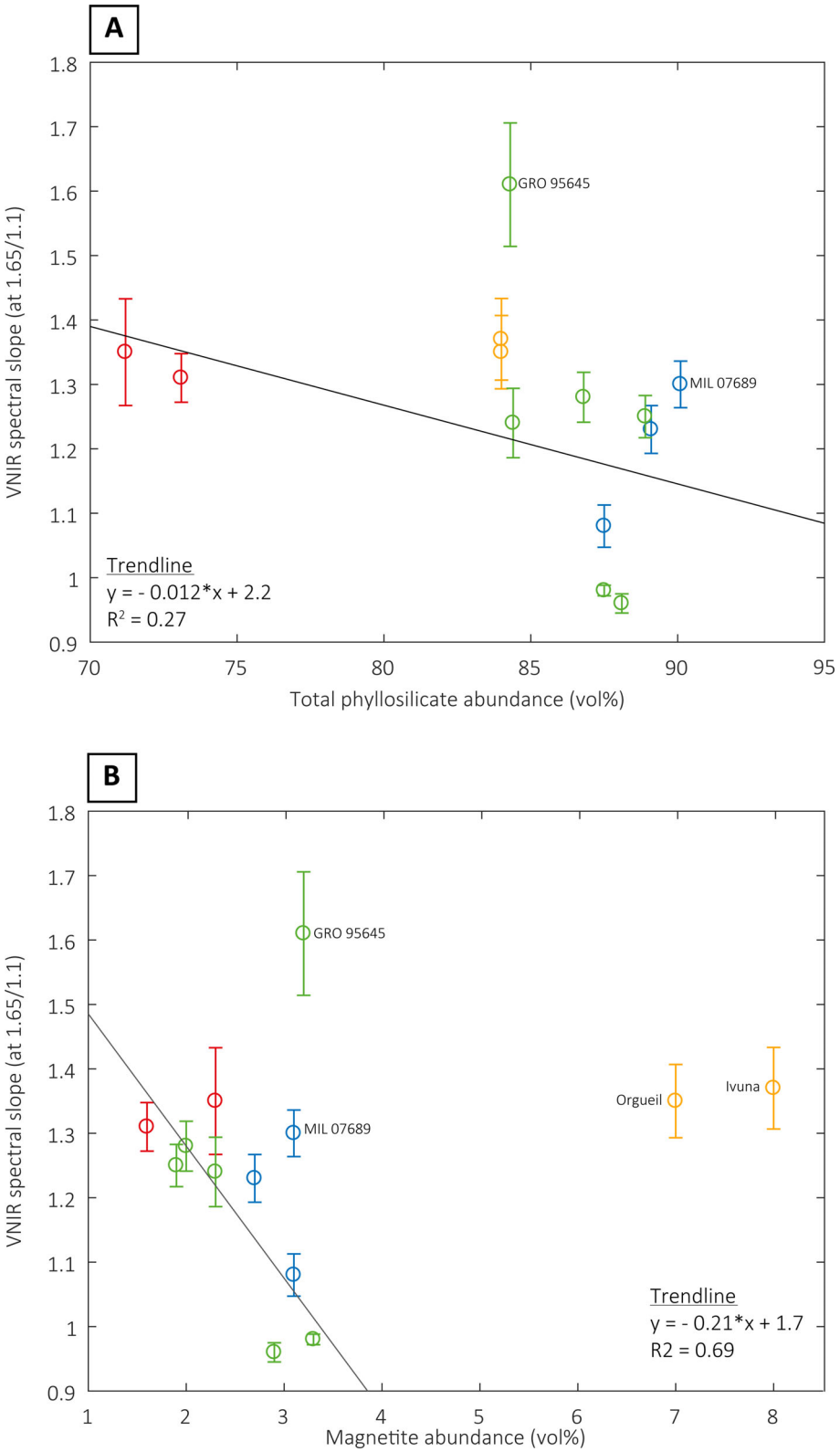

Fig. 7. VNIR spectral slope as calculated by the reflectance at 1.65 μm divided by the reflectance at 1.05 μm against (A) phyllosilicate abundance, and (B) magnetite abundance. Colors refer to the PSF petrologic types as described in Fig. 3. CI chondrites are in orange for clarity. The spectral slopes of the CM1/2 and CM1 chondrites decrease with increasing magnetite and phyllosilicate contents, which are both products of increasing degrees of aqueous alteration. GRO 95645 and MIL 07689 plot away from these trends because they contain Fe-(oxy)hydroxides formed during terrestrial weathering. The CI chondrites have unusually steep spectral slopes for their high magnetite abundance (~8 vol%). This may be due to the CIs having different physical properties to the CMs.

Ivuna by King et al. (2015a). It appears that the red spectral slopes we observe for the CIs are not reflecting mineralogy (e.g., high abundances of magnetite) and cannot easily be tied to composition. The difference in spectral trends between CM and CI chondrites might be related to physical properties, such as grain size or crystallinity, and requires further investigation.

While there is a trend of decreasing slope with increasing aqueous alteration in CM and CI chondrites, and a trend of decreasing slope with increasing magnetite content in the CM chondrites, the VNIR slope appears to be affected by weathering products, and based on this and its relationship to other physical properties such as grain size, we agree with the conclusions of McAdam et al. (2015) that it may not be the best spectral metric for determining mineralogy.

3 μm Feature

The 3 μm absorption is caused by the stretching, bending, and overtone vibrations of H_2O and the stretching vibration of OH^-. Water causes features near 3.1 μm, whereas the exact position of the feature caused by the OH^- depends on the cations to which those molecules are bound, and tends to be between 2.5 and 3.0 μm (Gaffey et al. 1993). The CM1/2, CM1, and CI1 chondrites are comprised mostly (~70 to 90 vol%) of serpentine-group phyllosilicates (King et al. 2015a; King et al. 2017), which contain OH^- anions bonded to Mg^{2+} and Fe^{2+} cations. We therefore expect the 3 μm feature in the spectra of the highly altered CM and CI chondrites to have shapes and positions similar to serpentine group phyllosilicate standards, and to vary depending on the composition of the phyllosilicates, which changes with increasing degrees of aqueous alteration.

Studies of the 3 μm region for CM and CI chondrites show a correlation between the position of the feature and the mineralogy of the meteorite. Beck et al. (2010, 2014) investigated transmission IR spectra of CM and CI chondrites and saw a shift to shorter wavelength of the 3 μm feature due to progressive enrichment of Mg in serpentine phyllosilicate minerals as the degree of aqueous alteration increased. This was also observed by Takir et al. (2013), who found that intermediately altered CM chondrites show spectral features consistent with Fe-cronstedtite and highly altered CM chondrites have spectral features which resemble Mg-serpentines. Note that both studies heated their samples prior to measurements to remove the effects of terrestrial adsorbed water.

The spectra of the CM1/2 chondrites MCY 05231 and LAP 031214 are similar to the spectra of the CM2 Murchison in the 3 μm region and are distinct from the other CM1/2 and CM1 chondrites: MCY 05231, LAP 031214, and Murchison spectra show rounded features at 2.78 – 2.82 μm (Fig. 3A). MCY 05231 and LAP 031214 are the least aqueously altered of the CM1/2 chondrites investigated here, containing the lowest phyllosilicate abundances (71 and 73 vol%, respectively). The composition of their phyllosilicates is more Fe-rich than the other CM1/2 and CM1s, with Mg-serpentine/Fe-cronstedtite ratios of 1.31 and 0.98 in comparison with >1.64. We suggest that the 3 μm features of MCY05231 and LAP 031214 therefore reflect the higher component of Fe-cronstedtite, the spectra of which has a feature at longer wavelengths than the more Mg-rich phyllosilicate species (Fig. 2B). King et al. (2017) suggested these two samples be reclassified as CM2 chondrites, and the similarity of their 3 μm features with that of the Murchison meteorite supports this conclusion. In the spectra of the more altered CM1/2s and CM1s, features at 2.73–2.74 μm correspond well with our Mg-serpentine standards, consistent with the more Mg-rich compositions of the phyllosilicates in these meteorites (Mg-serpentine abundances in these samples vary between 52 and 72 vol%).

Overall, we see a shift in the band center of the 3 μm feature from longer wavelengths in the samples with the lowest phyllosilicate abundances (e.g., LAP 031214 [71 vol%] and MCY 05231 [73 vol%]), to shorter wavelengths in the intensely altered samples with the highest phyllosilicate abundances (84–90 vol%). This shift occurs due to changes in phyllosilicate composition, with removal of heavier Fe^{2+} cations from the phyllosilicate structure, coupled with an increase in more Mg-rich phyllosilicate species, as total phyllosilicate abundance increases with progressive aqueous alteration (King et al. 2017). The shift to shorter wavelengths with increasing degrees of aqueous alteration is consistent with previous spectral results of CM chondrites, and likely a useful parameter for remotely inferring the mineralogy and aqueous alteration state of asteroid surfaces (Beck et al. 2010, 2014; Takir et al. 2013).

We find that the area of the asymmetrical 3 μm feature appears to be influenced by aqueous alteration extent in CM chondrites, with band area decreasing as total phyllosilicate abundance increases. This is likely caused by changes in phyllosilicate chemistry and increasing magnetite abundances as aqueous alteration proceeds. Qualitative examination of the CM chondrite spectra shows the 3 μm feature to be much broader than those of the Mg-serpentine phyllosilicate standards (note that standards were not heated prior to measurements). The initial 2.87 μm feature in the spectra of the Fe-cronstedtite standard is broader than the 2.72 μm in the Mg-serpentine, even despite the adsorbed water feature at 3.06 μm, and its calculated area over the range 2.67–3.85 is much larger than the feature in the Mg-serpentine standard spectra

(0.54 μm^{-1} in comparison to 0.32–0.37 μm^{-1}). Fe-cronstedtite therefore acts to increase 3 μm band area, and so the CM chondrites with the highest Fe-cronstedtite abundances have the largest areas, shown in Fig. 8A. Figure 8B shows that increasing magnetite content also correlates with decreasing band area, which is expected as magnetite is known to act as an opaque and can subdue features as its abundance increases (Cloutis et al. 1990). Therefore, the samples with highest magnetite contents show the smallest band areas. As discussed above, magnetite has been shown to increase with increasing aqueous alteration, and so this mineralogical change, coupled with decreasing Fe-cronstedtite abundances, acts to reduce 3 μm band area as aqueous alteration extent increases.

There are two outliers in Fig. 8, with very large 3 μm band areas: GRO 95645 and MIL 07689, which as discussed above, are the most terrestrially weathered meteorites analyzed in this study. TGA indicates that both contain terrestrial weathering products that would not be removed on heating to 150 °C and therefore still contribute to the 3 μm feature. The Fe-(oxy)hydroxide ferrihydrite, for example, has a strong absorption feature at ~3 μm (Bishop et al. 1993), and its presence could explain the larger band area in GRO 95645 and MIL 07689.

The 3 μm region in the CI chondrite spectra show two distinctive features (Fig. 4): a sharp absorption at 2.72 μm followed by a broader feature between 2.75 and 3.30 μm. Our Mg-serpentine and saponite standard spectra show a feature at 2.72 μm (Fig. 2B), suggesting the initial sharp feature is caused by Mg-OH, as with the feature in the same location in the CM1/2 and CM1 chondrites. The broad feature centered at 2.98 μm in the spectrum of Orgueil, and at 3.01 μm in the spectrum of Ivuna, is caused by H_2O. As the meteorite samples were heated to above 150 °C, we can assume this feature is not caused by terrestrially adsorbed water, rather bound interlayer water in the smectite phyllosilicates which was not removed on heating (Bishop et al. [1993] and references within). The contribution of ferrihydrite, which was found in Orgueil but not Ivuna (King et al. 2015a), is probably small due to the similarity between the spectral shape and position of the features in the CI spectra.

MIR Spectral Relationships to Mineralogy

6 μm Feature

The region between 5 and 7 μm can be difficult to disentangle in the spectra of CM and CI chondrites as it contains features that are related to the overtones and combination tones of Si-O in the anhydrous minerals as well as the bending of H_2O and -OH which are present in phyllosilicates (Salisbury et al. 1991; Lucey et al. 2017). We see features in this region in our phyllosilicate standard spectra (Fig. 2C), but also in the emissivity spectra of olivine (Fig. 2D). Beck et al. (2018) found an absorption feature in the IR reflectance spectra of all CM chondrites near 6 μm, and suggested it was due to interlayer H_2O in phyllosilicates or adsorbed water as samples were not heated prior to measurement. We observe features in this region in all the spectra of the CM2, CM1/2, CM1, and CI1 chondrites (Figs. 3 and 4). As our samples were heated prior to measurement, we believe the features here are related to mineralogy rather than adsorbed water.

The Fe-cronstedtite spectrum has a broad feature centered at 5.97 μm, while lizardite and antigorite show multiple features with maxima between 5.89 and 6.34 μm (Fig. 2C). The spectrum for the olivine standard also shows a doublet feature in this region, near 5.65 and 6.00 μm (Fig. 2D). The band centers in the CM1/2 and CM1 chondrite spectra plot within the range of those for the phyllosilicates, suggesting that the 6 μm feature is controlled by the phyllosilicates which dominate the bulk mineralogy of the meteorites, rather than the anhydrous olivine that is present in some of the samples. The spectra of Orgueil and Ivuna have broad 6 μm features with centers at 6.12 and 6.10 μm, respectively, and a shoulder at ~5.8 μm. These positions are similar to the spectra for the CM1/2 and CM1 chondrites and the phyllosilicate standards. The saponite spectrum in particular has a doublet feature with centers at 5.89 and 6.18 μm, and considering the phyllosilicates in CIs are a serpentine-saponite mixture (Bland et al. 2004), the 6 μm feature in the CI spectra might be a combination of the different phyllosilicate compositions.

Unlike the 3 μm region, there does not appear to be a trend in position of the 6 μm feature with mineralogy, likely because the features are complex and it is difficult to identify a trend even within the phyllosilicate endmember standards. As both the hydrated and anhydrous minerals have features in this region, it may not be a useful metric for establishing whether hydration has taken place.

Christiansen Feature

The CF in a mineral is caused by the real part of the refractive index approaching the refractive index of the surrounding material (in the case of this study, the surrounding medium is a vacuum and the refractive index is 1). As the way in which the refractive index changes with wavelength is unique to each mineral, the CF is unique to each mineral (Conel 1969). In meteorites, however, due to their complex mineralogy, single peaks representative of individual mineralogy are

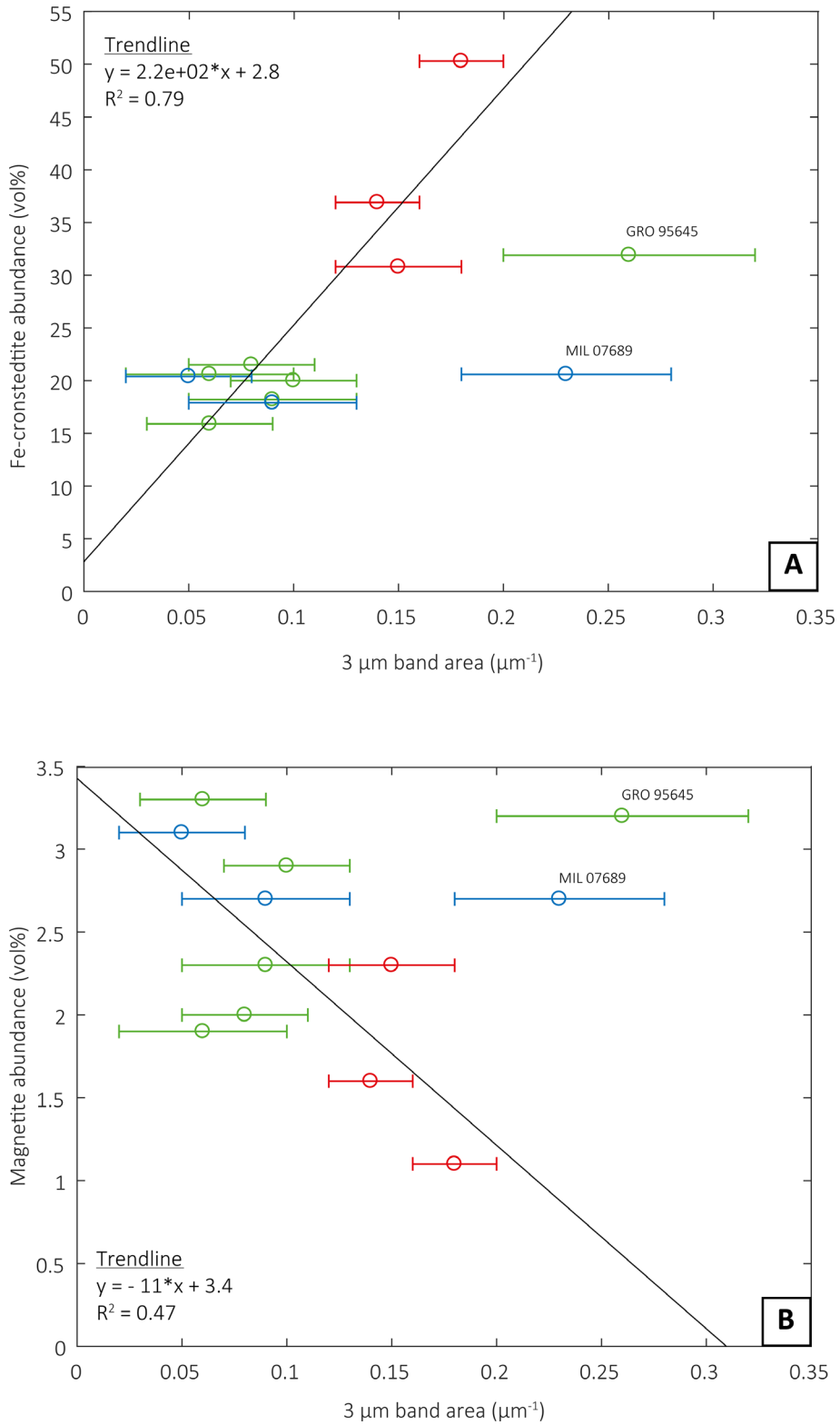

Fig. 8. Fe-cronstedtite abundance versus 3 µm band area (A) and magnetite abundance versus 3 µm band area (B) for the CM1/2 and CM1 chondrites. The 3 µm band area is correlated with both increasing with increasing Fe-cronstedtite and decreasing with increasing magnetite. The two outliers with larger band areas and lower Fe-cronstedtite abundances are MIL 07689 and GRO 95645, which are highly weathered and contain Fe-(oxy)hydroxides (see text for details).

difficult to identify (Salisbury et al. 1991). As a result, previous MIR studies of CM and CI chondrites have not observed systematic changes in CF position with bulk mineralogy (e.g., McAdam et al. 2015). However, McAdam et al. (2015) did report a change in the shape of the CF, with features becoming more distinct with increasing alteration.

All CFs in the spectra of the CM1/2 and CM1 chondrites are identified between 8.75 and 9.12 μm (Fig. 5). In Fig. 9, there is only a weak relationship (R^2 of 0.17) between the position of the CF and total phyllosilicate abundance, corroborating conclusions by McAdam et al. (2015). However, the intermediately altered MCY 05231 spectrum does have a CF at longer wavelengths (9.12 μm) and is similar to the CM2 Murchison spectrum (9.10 μm), whereas the CF in the other CM1/2 and CM1 chondrite spectra cluster between 8.75 and 9.06 μm (Fig. 9). Our Fe-cronstedtite spectrum has a CF at 9.66 μm and the Mg-serpentine CF is identified at 8.58 μm (Fig. 2C), and so this difference in CF position between intermediately and highly altered CMs could reflect changes in phyllosilicate composition, which becomes increasingly Mg-rich as aqueous alteration proceeds. Highly aqueously altered CM spectra have CFs at shorter wavelengths, due to higher Mg-serpentine abundances, and intermediately altered CM spectra have CFs at longer wavelengths, due to higher Fe-cronstedtite abundances. Within the highly altered CM spectra, there are no further trends in position of the CF, indicating that the CF position can only provide coarse resolution between mildly, intermediately, and highly altered meteorites.

The control of the phyllosilicate composition on the position of the CF is further emphasized by the position of the CF in the CM1/2 LAP 031214 spectrum. LAP 031214 has a similar mineralogy to MCY 05231 and Murchison (~20 vol% anhydrous silicates, ~70 vol% phyllosilicates) but a much sharper CF with a position at a shorter wavelength (8.98 μm). However, despite comparable total phyllosilicate abundances, the Mg-serpentine/Fe-cronstedtite ratio is higher for LAP 031214 (1.31) than MCY 05231 (0.98) and Murchison (0.44), suggesting that its phyllosilicates are more Mg-rich and it underwent a higher degree of aqueous alteration (King et al. 2017). The point at which Mg-serpentine abundance increases above Fe-cronstedtite abundance could represent a threshold at which Mg-serpentine begins to dominate the shape and position of the CF, and suggests phyllosilicate composition is a more important control than total phyllosilicate abundance on the position of the CF. This is in contrast to the 3 μm region, where the position of the feature is controlled more by total phyllosilicate abundance rather than composition. We therefore propose that as the degree of aqueous alteration increases in CM chondrites, the CF position shifts to shorter wavelengths before the 3 μm band shifts to shorter wavelengths, and the two features should be used in combination to constrain the extent of hydration. The relationship between these two features is shown in Fig. 10. In addition, we also find that the shape of the CF becomes sharper and distinct with increasing aqueous alteration. This is due to the increasing dominance of Mg-serpentine as alteration progresses, and extends the trend in CF shape first observed by McAdam et al. (2015).

The spectra of Orgueil and Ivuna have CFs at similar positions to the spectra of the highly altered CM chondrites, at 8.79 and 8.80 μm, respectively; however, the features are broader and a single peak is not distinguishable. Unlike the highly altered CMs, where the phyllosilicate composition is dominated by Mg-serpentine, the phyllosilicates in the highly altered CI1s are a serpentine-saponite mixture, and the CFs seen in their spectra are likely combinations of the CFs of these different phyllosilicates. The Mg-serpentine and saponite spectra have CFs near 8.58 and 8.21 μm, respectively, and with both present in the CI chondrites, it is difficult to identify a single diagnostic peak.

Transparency Feature

The TF is a reflectance maximum (emissivity minimum) between 11 and 13 μm that appears in spectra of fine-grained samples which have been found to correlate aqueous alteration. McAdam et al. (2015) identified a trend in the position of the TF peak in the spectra of CM and CI chondrites, with centers shifting to shorter wavelengths with increasing phyllosilicate abundance. They found less altered meteorites with lower phyllosilicate abundances had centers near 12.3 μm, and more altered with higher phyllosilicate abundances meteorites had centers near 11.4 μm. In addition, they found chondrites with intermediate levels of aqueous alteration showed a doublet feature. Additionally, Beck et al. (2018) found a correlation between the 12.4/11.4 reflectance ratio μm (which corresponds to an olivine feature) and water content in CM chondrites,

We see a similar trend, with the TFs shifting to shorter wavelengths with increasing total phyllosilicate abundance (Fig. 11A). However, the LAP 031214 spectra, as in the CF region, show a TF more consistent with the highly altered CM1/2 and CM1 chondrites, despite its mineralogy being similar to the intermediately altered Murchison and MCY 05231. We propose the TF, like the CF, is also affected by phyllosilicate composition in addition to total phyllosilicate abundance. This can be demonstrated by the trend between TF position and the Mg-serpentine/Fe-cronstedtite ratio of the phyllosilicates in the CM chondrites (Fig. 11B), with the TF shifting to

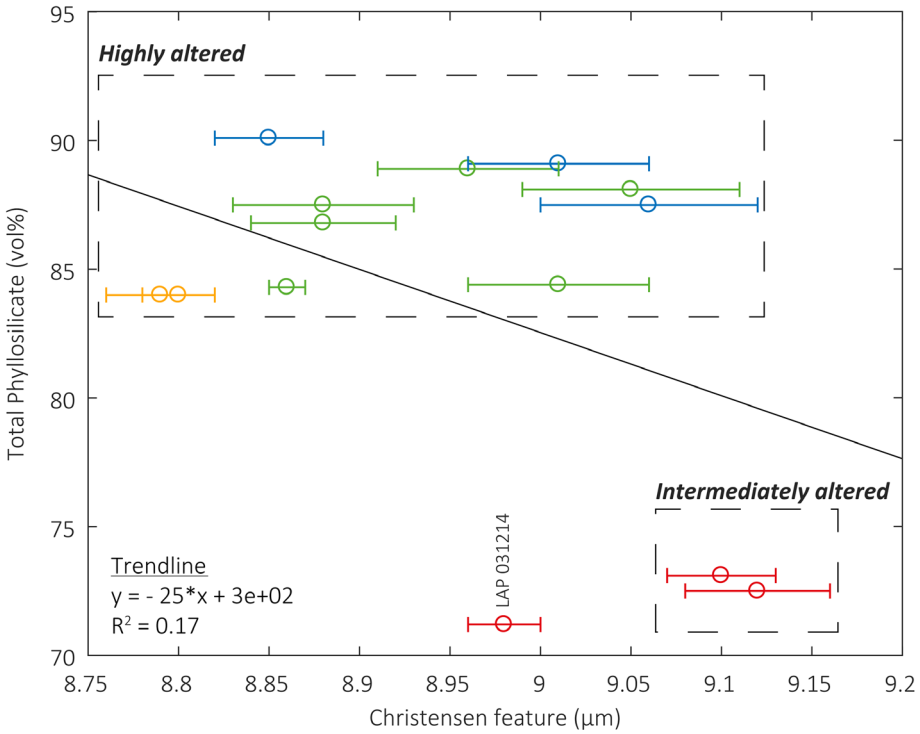

Fig. 9. Total phyllosilicate abundance in CM2, CM1/2, CM1, and CI1 chondrites versus the position of the Christiansen feature (CF) in MIR spectra. There is only a weak relationship between position and phyllosilicate abundance, but intermediately altered CMs seem to cluster at longer wavelengths than the highly altered CMs and CIs. LAP 031214 is anomalous due to its Mg-rich phyllosilicate composition (see text for details).

shorter wavelengths as Mg-serpentine (TF at ~11.64 μm) becomes more abundant than Fe-cronstedtite (TF at 12.28 μm). This ratio is highest in the most altered CM chondrites as phyllosilicates get progressively more Mg-rich with aqueous alteration (King et al. 2017). The spectra of the CM2 chondrite Murchison and the CM1/2 MCY 05231, which have the lowest Mg-serpentine/Fe-cronstedtite ratios, have TF features at the longest wavelengths (12.51 and 12.31 μm), which additionally correspond with the positions of the TF in the spectra of the least altered samples investigated by McAdam et al. (2015). These positions could additionally also be influenced by the higher abundance of olivine (15 vol% in Murchison and 20 vol% in MCY 05231), the spectrum of which shows a TF at 12.90 μm (Fig. 2D).

The spectra of the highly altered CI chondrites Orgueil and Ivuna follow the same trend, with TF positions (11.58 and 11.56 μm) shifted to shorter wavelengths (Fig. 11A). The similarity of the TFs in the spectra of Orgueil and Ivuna to those in the spectra of the most altered CM chondrites suggests the TF might be a useful parameter in assessing the degree of aqueous alteration across different chondrite groups and in remote sensing observations of asteroids with fine particulate surfaces. This is in contrast with the variation in the shape and position of the CF between the most aqueously altered CM chondrites and CI chondrites.

There is a correlation between TF position and phyllosilicate abundance, although composition of the phyllosilicates also plays a role. For the highly aqueously altered chondrites, the TFs are identified at short wavelengths (11.36–11.95 μm), whereas for the intermediately and mildly altered samples, they occur at longer wavelengths (12.51 and 12.31 μm). Both the CF and TF are more sensitive to the phyllosilicate composition than the VNIR spectral slope and 3 μm features, so using both in conjunction can help constrain the extent of aqueous alteration.

Spectral Parameters for Mineral Identification

We have examined a number of parameters in the VNIR and MIR spectra of CM and CI chondrites and established how they vary with mineralogy. The VNIR slope is sensitive to several physical properties (e.g., grain size) of a sample, but if these are well characterized, variations in the slope can be tied to the opaque content of a meteorite. In the CM chondrites, spectral slope decreases with increasing magnetite content (Fig. 7B), which reflects the extent of aqueous alteration.

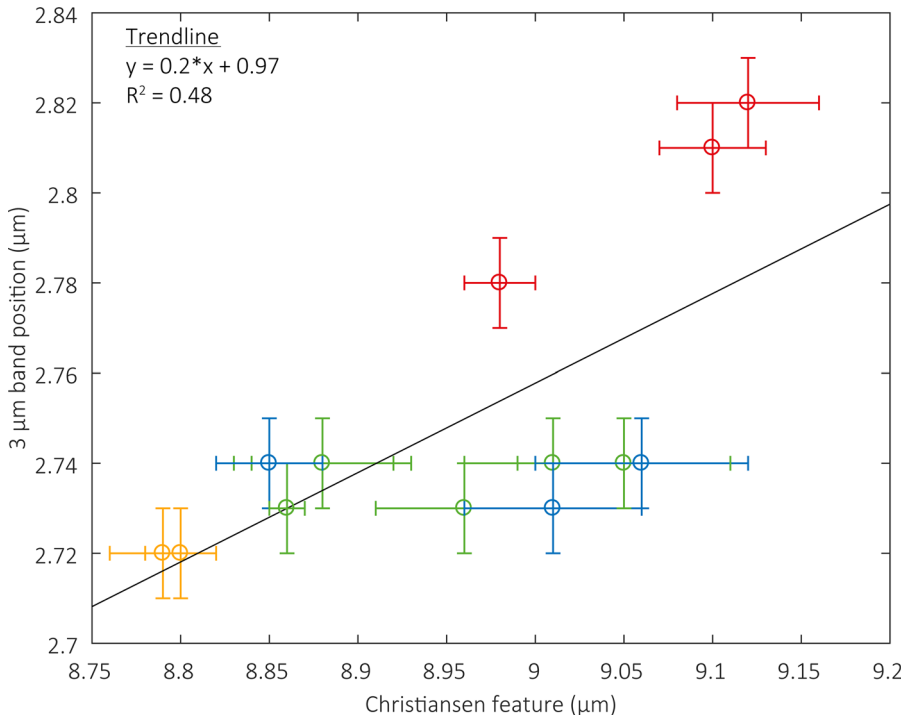

Fig. 10. The position of the 3 μm feature and its relationship to the position of the CF. These two features can be used in conjunction to constrain aqueous alteration extent, as shifts in feature position are caused by different mechanisms: the 3 μm position is controlled by total phyllosilicate abundances, and the CF is controlled changes in phyllosilicate chemistry. As the graph suggests, the CM1/2 LAP 031214 is likely more aqueously altered than the CM1/2 MCY 05231 and the CM2 Murchison.

Furthermore, there is a reasonable trend between spectral slope and phyllosilicate abundance of the CM chondrites (Fig. 7A). The 6 μm feature appears to be indicative of hydration in CM and CI chondrites; however, there is no trend with mineralogy or extent of alteration, and as this region also has contributions from anhydrous silicates, it is complex to disentangle composition. The 3 μm feature, CF and TF show trends related to the degree of aqueous alteration, with all three parameters shifting to shorter wavelengths with increasing hydration. In particular, the position and shape of the 3 μm feature are useful: intermediately altered CMs have rounded features at ~2.8 μm, and with increasing aqueous alteration these features become sharper and shift to shorter wavelengths. This is related to increasing phyllosilicate abundance, an increasing amount of which is Mg-serpentine. Additionally, we suggest that band area may decrease with increasing aqueous alteration due to decreasing Fe-cronstedtite and increasing magnetite. The CF and TF are more sensitive to phyllosilicate composition, shifting to shorter wavelengths as the Mg-serpentine/Fe-cronstedtite ratio of the phyllosilicates increases. As both total phyllosilicate abundance and Mg-serpentine phyllosilicate abundance are related to aqueous alteration extent, all three spectral parameters can be used to constrain the alteration history of a sample.

Asteroid Comparisons

Telescopic observations of asteroids from the ground are hampered by the effect of telluric absorption by gases in the atmosphere; ozone (which has features at 0.35 μm and at 9.6 μm), carbon dioxide (2.01, 2.06, and 1.6 μm), and water vapor (multiple features throughout the spectrum, including a significant one near 3 μm; Rivkin et al. 2015; Burbine 2017). This issue can mask features related to minerals present on the asteroid. Some wavelength ranges, such as the TF region, fall into "atmospheric windows," meaning they are observable by ground-based instruments. These are therefore important to investigate in order to evaluate alteration on asteroid surfaces from the ground.

To remedy this, some space-based telescopes also observe asteroids in the VNIR and MIR, for example, the Spitzer Space Telescope and the Akari infrared astronomy satellite (Houck et al. 2004; Murakami et al. 2007; Licandro et al. 2012; Marchis et al. 2012; Lim et al. 2019). However, when remotely observing asteroids using these telescopes, spectral flux above

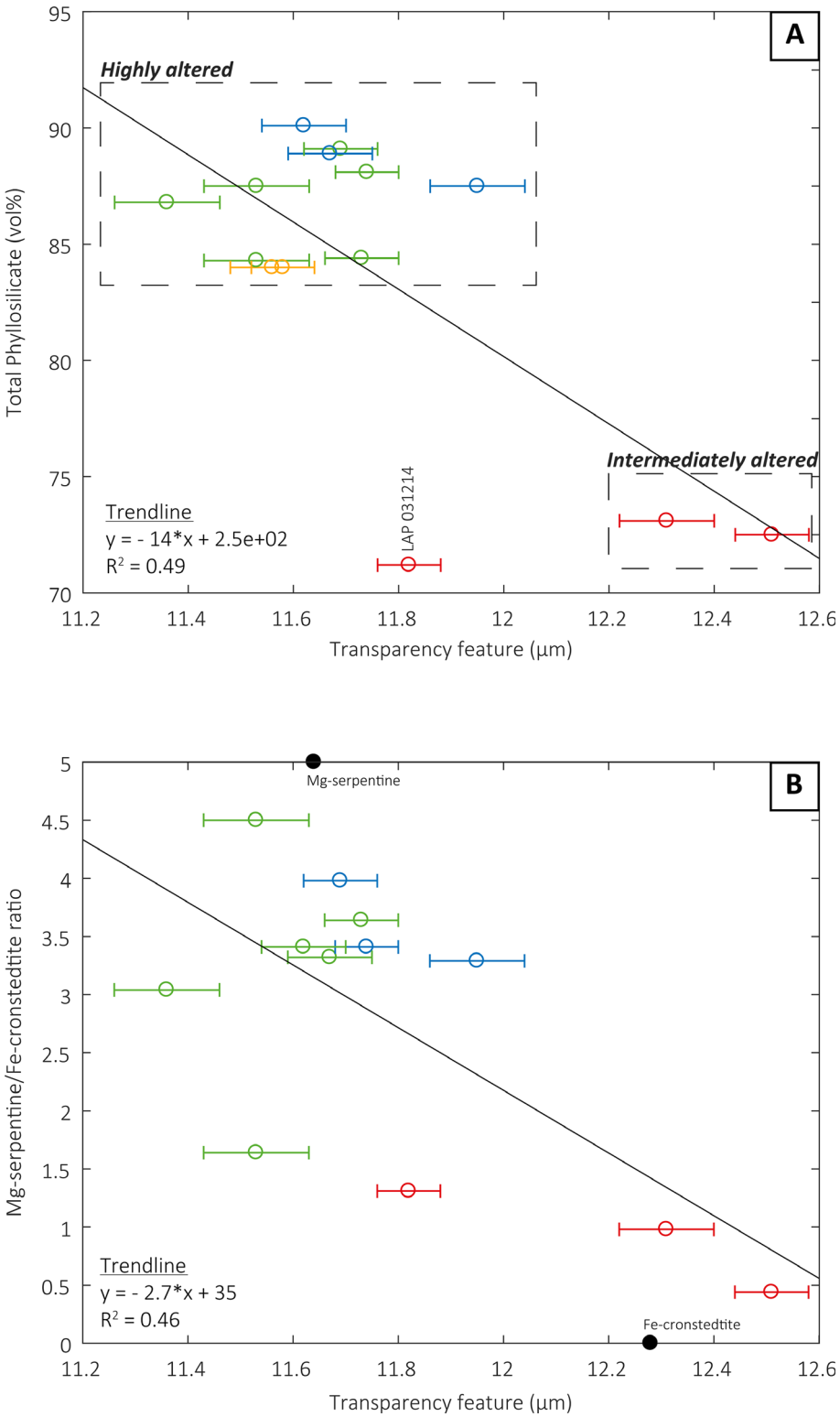

Fig. 11. The position of the TF in the CM2, CM1/2, CM1, and CI1 chondrite spectra and its relationship to total phyllosilicate abundance (A) and the Mg-serpentine/Fe-cronstedtite ratio of the phyllosilicates (B). Note that in 10(A), CI chondrites are in orange, and in 10(B), they are not included. Both total phyllosilicate abundance and phyllosilicate composition show a relationship to the position of the TF, with the feature shifting to shorter wavelengths with increasing phyllosilicate abundance, and a change to more Mg-rich phyllosilicate. Both are associated with higher degrees of aqueous alteration.

~5 μm is dominated by thermal emission, rather than reflectance (Salisbury 1993), and it is difficult to interpret emissivity data with reflectance measurements (e.g., Donaldson Hanna et al. 2019). The observed spectral energy is controlled by the size, composition, and temperature distribution of the body, which is in turn strongly affected by factors such as heliocentric distance, albedo, thermal inertia, physical properties (e.g., particle grain size of the regolith), and rotation rate (e.g., Emery et al. 2006). Despite this, reflectance measurements can be compared to emission spectra using Kirchhoff's law: $E = 1 - R$, where E is emissivity and R is reflectance. However, this is only accurate when hemispherical reflectance is used. In this study, a bidirectional spectrometer setup was used, but it has been demonstrated that spectral differences between hemispherical and bidirectional reflectance are observed in magnitude of features, but not in feature position, so qualitative comparisons can be made between reflectance and emissivity (Salisbury et al. 1991; Salisbury 1993). For example, McAdam et al. (2015) compared the emissivity spectra of the C-/B-type asteroid (24) Themis collected by the Spitzer Space Telescope Infrared Spectrograph (IRS) to the reflectance spectra of CM chondrites. Themis has previously been related to CM and CI chondrites based on its VNIR spectra between 0.4 and 2.5 μm (Clark et al. 2010), and may have water ice on its surface (Rivkin and Emery 2010). McAdam et al. (2015) found the position of the TFs in the spectra of Themis to be most similar to those for the CM2 chondrite QUE 97990 (this comparison was only near the TF, however, and in the full spectral range the similarities are less robust).

In addition to space telescope observations, we also have data collected from spacecraft orbiting asteroids. Figure 12 shows the average spectrum of Ceres between 1 and 4.3 μm, collected by the DAWN spacecraft (De Sanctis et al. 2015, 2018). There is a broad asymmetric feature observed between 2.6 and 4.2 μm with a number of distinct absorption features at 2.72, 3.05–3.1, 3.3–3.5, and 3.95 μm. De Sanctis et al. (2018) attributed these to OH^-, NH_4^+, organics, and CO_3^-, respectively. Particularly relevant to this study is the position of the sharp feature at 2.72 μm, which is indicative of Mg-OH phyllosilicate species. This could result from Mg-serpentine, which is the most abundant phase in the highly altered CM1 chondrites, or saponite, which is a major phase in the CI1 chondrites. To date, Ceres has mainly been compared to the spectra of CM2 and CI1 chondrites (McSween et al. 2017; De Sanctis et al. 2018), partly due to the limited number of IR spectra available for CM1/2 and CM1 chondrites. Figure 12A shows the spectrum of Ceres and the spectrum of CM2-like MCY 05231 and the CI1 Orgueil, and in contrast Fig. 12B compares the 3 μm feature of Ceres with the most altered (and not extensively weathered) CM1 chondrite MIL 05137. The features at ~2.72 μm in the Ceres and MIL 05137 spectra are similar and appear to be better matched than Ceres and MCY 05231 and Orgueil, both in position and spectral shape below ~2.95 μm. This suggests that materials on the surface of Ceres are CM1-like, having experienced extensive aqueous alteration, and supports the conclusions of McSween et al. (2017).

The feature at 3.07 μm has been hypothesized to be caused by ammoniated phyllosilicates (De Sanctis et al. 2015). As with other measurements of the 3 μm region of carbonaceous chondrites, we do not see this feature in our meteorites. This has been suggested by De Sanctis et al. (2018) to be due to different processes occurring on the parent body of our meteorites, or potentially a different formation scenario for Ceres. Despite this, the presence of Mg-OH phyllosilicate species does indicate a high extent of aqueous alteration on Ceres and may indicate some similarities between it and the parent body of the CM1 chondrites.

In comparisons above 5 μm, however, the similarity between Ceres and the highly altered CM1 chondrites is less robust. Vernazza et al. (2017) show a spectrum of Ceres between 5 and 12 μm, as collected by the Stratospheric Observatory for Infrared Astronomy (SOFIA) and the Infrared Space Observatory (ISO), and identify emissivity features near 7 and 10 μm, the latter of which has two peaks at 9.8 and 10.65 μm. This is consistent with previous measurements of Ceres using the NASA IRTF (Milliken and Rivkin 2009). All meteorites in this study show CFs at shorter wavelengths, and additionally, none show as significant a feature at 7 μm as the Ceres spectrum, which has been suggested to be due to carbonates or ammoniated phyllosilicates (Vernazza et al. 2017). This suggests that the highly aqueously altered CM chondrites may only be a partial spectral match to Ceres and highlights the importance of using multiple wavelength ranges during analysis.

Hayabusa2 and OSIRIS-REx both have instruments on board which cover some of the wavelength ranges investigated here. In the VNIR, Hayabusa2 has on its main spacecraft the Near-Infrared Spectrometer (NIRS3, the "3" comes from the 3 μm feature), which covers the range 1.8–3.2 μm (Iwata et al. 2017). OSIRIS-REX has the OSIRIS-REx Visible Infrared Spectrometer (OVIRS), which operates over the range 0.4–4.3 μm (Reuter et al. 2018). Both missions also have instruments which operate at longer wavelengths: the MASCOT Radiometer (MARA) has a series of channels, some of which should observe some of the features described here (5.5–7 μm, 8–9.5 μm, and 9.5–11.5 μm; Grott et al. 2017) and OSIRIS-REx has the

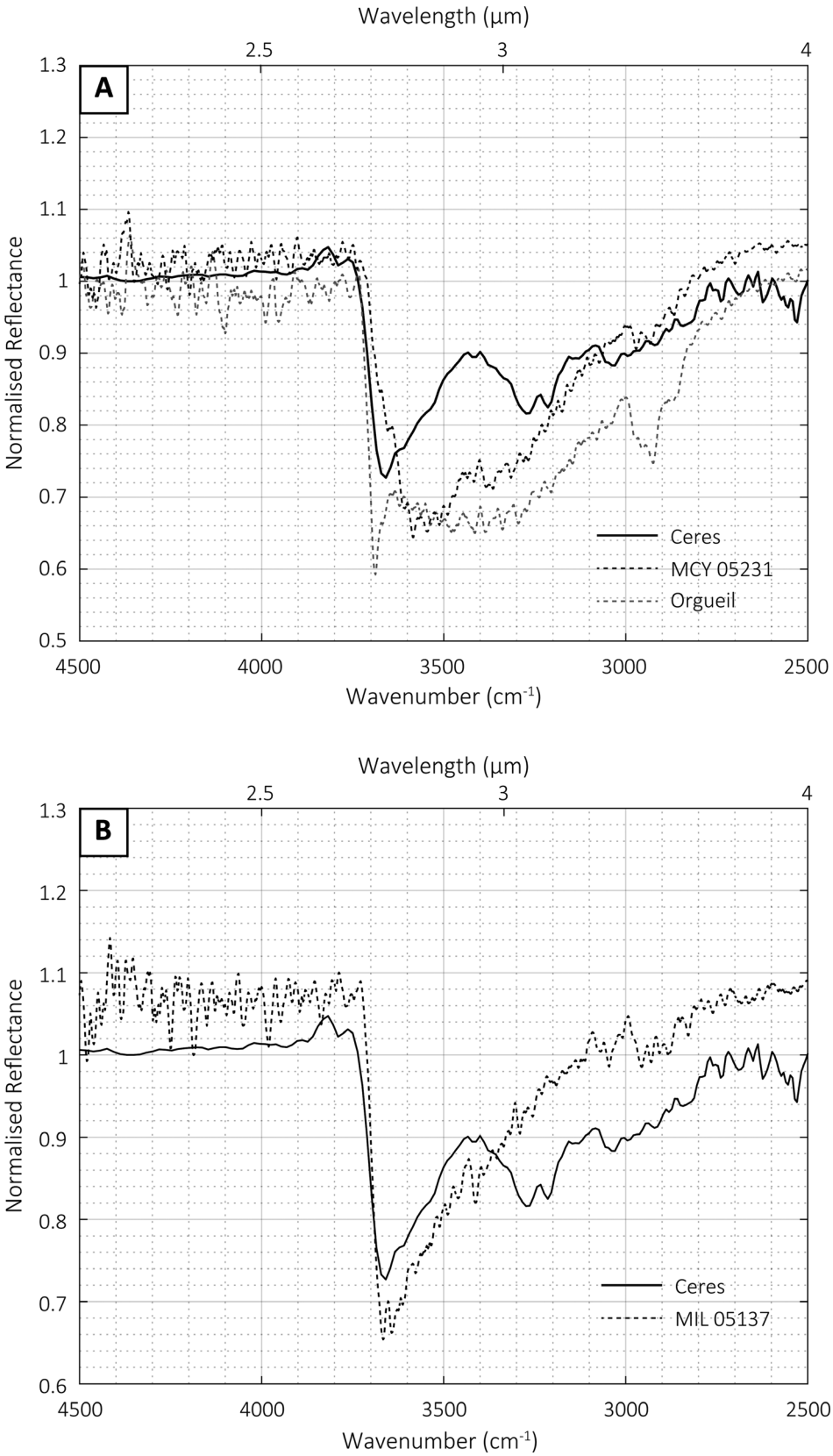

Fig. 12. The 3 μm feature of 1 Ceres compared to the CM1/2 MCY 05231, which has been suggested to be more CM2-like (A), the CI1 chondrite Orgueil (A) and the CM1 chondrite MIL 05137 (B). The 1 Ceres spectrum is from De Sanctis et al. (2018). All spectra are normalized to unity at 2.3 μm.

OSIRIS-REx Thermal Emission Spectrometer (OTES), which covers ~5 to 50 μm (Christensen et al. 2018).

Preliminary results from Hayabusa2 suggest that Ryugu resembles thermally metamorphosed CM/CI-like material, or has some similarities to interplanetary dust particles (Kitazato et al. 2019), and observations from OSIRIS-REx suggest that Bennu may be highly altered and CM1 and/or CI-like (Hamilton et al. 2019). The NIRS3 spectra from Ryugu show a single feature at 2.72 μm, but no features associated with H_2O-bearing minerals, or any NH_4-bearing phyllosilicates as inferred on the surface of Ceres (Kitazato et al. 2019). The feature is very shallow and thought to represent thermal dehydration. The position of the feature in the Ryugu spectrum corresponds well to the position of the feature caused by Mg-OH in our highly altered CMs and CIs. What happen to these spectral features when CM1s and CI1s are thermally dehydrated needs to be investigated further before the surface composition of Ryugu can be refined. The OVIRS data show a spectrum for Bennu with a feature at 2.74 μm and blue slope between 0.4 and 2.4 μm (Hamilton et al. 2019). The 2.74 μm feature is deeper than that of Ryugu, suggesting it has undergone very little, or no thermal dehydration. The position of the 2.74 μm feature corresponds well with the features seen in our highly altered CM1 and CM1/2 chondrites, and the blue slope suggests some magnetite is present. The OTES spectrum of Bennu shows an emissivity peak near 9 μm (Hamilton et al. 2019), which is also similar to the position of the CF in the spectra of our highly altered CM chondrites. Our measurements corroborate those of Hamilton et al. (2019) that materials on the surface of Bennu are CM1-like in nature.

CONCLUSIONS

Visible and near-infrared and MIR spectra of aqueously altered meteorites can help to ground truth remote observations of primitive, water-rich asteroids and infer their formation and evolution in the early solar system. To date, most spectral studies have focussed on the partially altered petrologic type 2 CM chondrites; here we present VNIR and MIR spectra for the highly altered CM1/2, CM1, and CI1 chondrites and describe identified trends related to their composition and the degree of secondary processing.

The VNIR slope between 1–1.1 μm and 1.6–1.7 μm decreases as both phyllosilicate and magnetite abundances increase with degree of aqueous alteration. In CM chondrites, the relationship between VNIR spectral slope and magnetite abundance is significantly stronger than that for phyllosilicates, suggesting that magnetite content is the main control in this spectral range. However, the VNIR spectral slopes for CI chondrites do not reflect their high magnetite abundances, implying that physical properties (such as grain size) also influence the spectra in this region. In addition, we confirm that terrestrial weathering causes a reddening of the VNIR slope. These factors combined suggest that the VNIR spectral slope is a challenging parameter for determining mineralogy.

The 3 μm feature shifts from centers near 2.80 μm in the intermediately altered CM chondrites to near 2.73 μm in the highly aqueously altered CMs. The CI chondrites also show a feature near 2.72 μm. This feature at shorter wavelengths is due to the presence of Mg-OH, consistent with a higher abundance of Mg-rich phyllosilicate phases in the highly hydrated chondrites. This shift to shorter wavelengths occurs as total phyllosilicate abundance increases, an increasing portion of which is Mg-serpentine.

The TF and CF in spectra of CM and CI chondrites both shift to shorter wavelengths as the degree of aqueous alteration increases. These features are sensitive to mineral composition, and are related to the Mg-serpentine/Fe-cronstedtite ratio of the phyllosilicates. The TF in particular shows a strong trend, with the feature shifting to shorter wavelengths as the phyllosilicate composition becomes more Mg-rich. The TF and CF are more sensitive to this Mg-enrichment than the 3 μm feature, and changes in position of the TF and CF occur at an earlier stage of aqueous alteration. This suggests that all three spectral parameters should be used in conjunction to constrain the processing experienced by meteorites and asteroid parent bodies.

The results presented here can be used to interpret remote observations of asteroids, and can help determine surface mineralogy and the degree of aqueous alteration. For example, spectra collected by the DAWN mission to (1) Ceres show a feature near 2.72 μm, which is very similar in shape and position to the same feature in the highly altered CM1 chondrites, suggesting the presence of abundant Mg-serpentine on the surface and near-complete aqueous alteration. Furthermore, comparisons of our data to the preliminary results from Hayabusa2 and OSIRIS-REx suggest that the CM1 chondrites may also be analogous to the surfaces of asteroids Ryugu and Bennu. Additionally, our results will be useful in evaluating previous Earth- and space-based telescopic observations and future solar system observations by the James Webb Telescope (Gardner et al. 2006). If trends related to mineralogy can be identified in remote spectral data, then conclusions can be drawn about the geological history of primitive bodies such as Ryugu and Bennu.

Acknowledgments—U.S. Antarctic meteorite samples are recovered by the Antarctic Search for Meteorites

(ANSMET) program which has been funded by NSF and NASA, and characterized and curated by the Department of Mineral Sciences of the Smithsonian Institution and Astromaterials Curation Office at NASA Johnson Space Center. Hot desert meteorite samples were provided by Laurence Garvie at the Center for Meteorite Studies, Arizona State University, USA. We thank Paul Schofield for analysis advice, and Maria Cristina De Sanctis for providing the spectrum of Ceres. We are grateful to Ed Cloutis and Pierre Beck for comments and reviews which greatly improved this manuscript. This work was supported by the Science and Technology Facilities Council (STFC), UK, through grant 1860431.

Editorial Handling—Dr. Edward Cloutis

REFERENCES

Alexander C. M. O'D., Bowden R., Fogel M. L., Howard K. T., Herd C. D. K., and Nittler L. R. 2012. The provenances of asteroids, and their contributions to the volatile inventories of the terrestrial planets. *Science* 337:721–723.

Barrat J.-A., Zanda B., Moynier F., Bollinger C., Liorzou C., and Bayon G. 2012. Geochemistry of CI chondrites: Major and trace elements, and Cu and Zn Isotopes. *Geochimica et Cosmochimica Acta* 83:79–92.

Battandier M., Bonal L., Quirico E., Beck P., Engrand C., Duprat J., and Dartois E. 2018. Characterization of the organic matter and hydration state of Antarctic micrometeorites: A reservoir distinct from carbonaceous chondrites. *Icarus* 306:74–93.

Beck P., Quirico E., Montes-Hernandez G., Bonal L., Bollard J., Orthous-Daunay F.-R., Howard K. T., Schmitt B., Brissaud O., Deschamps F., Wunder B., and Guillot S. 2010. Hydrous mineralogy of CM and CI chondrites from infrared spectroscopy and their relationship with low albedo asteroids. *Geochimica et Cosmochimica Acta* 74:4881–4892.

Beck P., Garenne A., Quirico E., Bonal L., Montes-Hernandez G., Moynier F., and Schmitt B. 2014. Transmission infrared spectra (2-25 μm) of carbonaceous chondrites (CI, CM, CV-CK, CR, C2 ungrouped): Mineralogy, water, and asteroidal processes. *Icarus* 229:263–277.

Beck P., Maturilli A., Garenne A., Vernazza P., Helbert J., Quirico E., and Schmitt B. 2018. What is controlling the reflectance spectra (0.35–150 μm) of hydrated (and dehydrated) carbonaceous chondrites? *Icarus* 313:124–138.

Bishop J. L., Pieters C. M., and Burns R. G. 1993. Reflectance and Mössbauer spectroscopy of ferrihydrite-montmorillonite assemblages as Mars soil analog materials. *Geochimica et Cosmochimica Acta* 57:4583–4595.

Bland P. A., Cressey G., and Menzies O. N. 2004. Modal mineralogy of carbonaceous chondrites by X-ray diffraction and Mössbauer spectroscopy. *Meteoritics & Planetary Science* 39:3–16.

Brearley A. J. 2006. The action of water. In *Meteorites and the early solar system II*, edited by Lauretta D. S. and McSween H. Y. Tucson, Arizona: The University of Arizona Press. pp. 587–624.

Burbine T. H. 2017. *Asteroids: Astronomical and geological bodies*. Cambridge, UK: Cambridge University Press.

Burbine T. H., McCoy T. J., Meibom A., Gladman B., and Keil K. 2002. Meteoritic parent bodies: Their number and identification. In *Asteroids III*, edited by Bottke W. F., Cellino A., Paolicchi P., and Binzel R. P. Tucson, Arizona: University of Arizona Press. pp. 653–667.

Christensen P. R., Hamilton V. E., Mehall G. L., Pelham D., O'Donnell W., Anwar S., Bowles H., Chase S., Fahlgren J., Farkas Z., Fisher T., James O., Kubik I., Lazbin I., Miner M., Rassas M., Schulze L., Shamordola K., Tourville T., West G., Woodward R., and Lauretta D. 2018. The OSIRIS-REx Thermal Emission Spectrometer (OTES) instrument. *Reviews Space Science* 214:87.

Clark B. E., Ziffer J., Nesvorny D., Campins H., Rivkin A., Hiroi T., Barucci M. A., Binzel R., Fornasier S., DeMeo F., and Ockert-Bell M. 2010. Spectroscopy of B-type asteroids: Subgroups and meteorite analogs. *Journal of Geophysical Research: Planets* 115:1–22.

Clark R. N. 1999. Spectroscopy of rocks and minerals, and principles of spectroscopy. In *Manual of remote sensing, volume 3, remote sensing for the Earth sciences*. New York: John Wiley and Sons, Inc. pp. 3–58.

Clayton R. N. and Mayeda T. K. 1984. The oxygen isotope record in Murchison and other carbonaceous chondrites. *Earth and Planetary Science Letters* 67:151–161.

Clayton R. N., and Mayeda T. K. 1999. Oxygen isotope studies of carbonaceous chondrites. *Geochimica et Cosmochimica Acta* 63:2089–2104.

Cloutis E. A., Gaffey M. J., Smith D. G. W., and Lambert R. S. J. 1990. Reflectance spectra of mafic silicate-opaque assemblages with applications to meteorite spectra. *Icarus* 84:315–333.

Cloutis E. A., Hiroi T., Gaffey M. J., Alexander C. M. O., and Mann P. 2011a. Spectral reflectance properties of carbonaceous chondrites: 1. CI chondrites. *Icarus* 212:180–209.

Cloutis E. A., Hudon P., Hiroi T., Gaffey M. J., and Mann P. 2011b. Spectral reflectance properties of carbonaceous chondrites: 2 CM chondrites. *Icarus* 216:309–346.

Conel J. E. 1969. Infrared emissivities of silicates' experimental results and a cloudy atmosphere model of spectral emission from condensed particulate mediums. *Journal of Geophysical Research* 74:1614–1634.

Cooper B. L. 2002. Midinfrared spectral features of rocks and their powders. *Journal of Geophysical Research* 107:1–17.

DeMeo F. E., Binzel R. P., Slivan S. M., and Bus S. J. 2009. An extension of the Bus asteroid taxonomy into the near-infrared. *Icarus* 202:16–180.

De Sanctis M. C., Ammannito E., Raponi A., Marchi S., McCord T. B., McSween H. Y., Capaccioni F., Capria M. T., Carrozzo F. G., Ciarniello M., Longobardo A., Tosi F., Fonte S., Formisano M., Frigeri A., Giardino M., Magni G., Palomba E., Turrini D., Zambon F., Combe J. P., Feldman W., Jaumann R., McFadden L. A., Pieters C. M., Prettyman T., Toplis M., Raymond C. A., and Russell C. T. 2015. Ammoniated phyllosilicates with a likely outer solar system origin on (1) Ceres. *Nature* 528:241–244.

De Sanctis M. C., Ammannito E., Carrozzo F. G., Ciarniello M., Giardino M., Frigeri A., Fonte S., McSween H. Y., Raponi A., Tosi F., Zambon F., Raymond C. A., and Russell C. T. 2018. Ceres's global and localized mineralogical composition determined by Dawn's Visible and Infrared Spectrometer (VIR). *Meteoritics and Planetary Science* 22:1–22.

Donaldson Hanna K. L., Thomas I. R., Bowles N. E., Greenhagen B. T., Pieters C. M., Mustard J. F., Jackson C. R. M., and Wyatt M. B. 2012. Laboratory emissivity

measurements of the plagioclase solid solution series under varying environmental conditions. *Journal of Research Geophysical: Planets* 117:1–7.

Donaldson Hanna K. L., Schrader D. L., Cloutis E. A., Cody G. D., King A. J., McCoy T. J., Applin D. M., Mann J. P., Bowles N. E., Brucato J. R., Connolly H. C. Jr., Dotto E., Keller L. P., Lim L. F., Clark B. E., Hamilton V. E., Lantz C., Lauretta D. S., Russell S. S., and Schofield P. F. 2019. Spectral characterization of analog samples in anticipation of OSIRIS-REx's arrival at Bennu: A blind test study. *Icarus* 319:701–723.

DuFresne E. R. and Anders E. 1962. On the chemical evolution of the carbonaceous chondrites. *Geochimica et Cosmochimica Acta* 26:1085–1114.

Emery J. P., Cruikshank D. P., and Van Cleve J. 2006. Thermal emission spectroscopy (5.2-38 μm) of three Trojan asteroids with the Spitzer Space Telescope: Detection of fine-grained silicates. *Icarus* 182:496–512.

Endress M., Zinner E. K., and Bischoff A. 1996. Early aqueous activity on primitive meteorite parent bodies. *Nature* 379:701–703.

Gaffey S. J., McFadden L. A., Nash D., and Pieters C. M. 1993. Ultraviolet, visible, and near-infrared reflectance spectroscopy: Laboratory spectra of geologic materials. In *Remote geochemical analysis: Elemental and mineralogical composition*, edited by Pieters C. M. and Englert P. A. Cambridge, UK: Cambridge University Press. pp. 43–79.

Gardner J. P, Mather J. C., Clampin M., Doyon R., Greenhouse M. A., Hammel H. B., Hutchings J. B., Jakobsen P., Lilly S. J., Long K. S., Lunine J. I., Mccaughrean M. J., Mountain M., Nella J., Rieke G. H., Rieke M. J., Rix H.-W., Smith E. P., Sonneborn G., Stiavelli M., Stockman H. S., Windhorst R. A., and Wright G. S. 2006. The James Webb space telescope. *Space Science Reviews* 123:485–606.

Garenne A., Beck P., Montes-Hernandez G., Chiriac R., Toche F., Quirico E., Bonal L., and Schmitt B. 2014. The abundance and stability of "water" in type 1 and 2 carbonaceous chondrites (CI, CM and CR). *Geochimica et Cosmochimica Acta* 137:93–112.

Greenberg R. and Chapman C. R. 1983. Asteroids and meteorites: Parent bodies and delivered samples. *Icarus* 55:455–481.

Grossman J. N. 1998. The Meteoritical Bulletin, No. 82. *Meteoritics & Planetary Science* 33:A221–A239.

Grott M., Knollenberg J., Borgs B., Hänschke F., Kessler E., Helbert J., Maturilli A., and Müller N. 2017. The MASCOT radiometer MARA for the Hayabusa 2 mission. *Space Science Reviews* 208:413–431.

Guo W. and Eiler J. M. 2007. Temperatures of aqueous alteration and evidence for methane generation on the parent bodies of the CM chondrites. *Geochimica et Cosmochimica Acta* 71:5565–5575.

Hamilton V. E., Simon A. A., Christensen P. R., Reuter D. C., Clark B. E., Barucci M. A., Bowles N. E., Boynton W. V., Brucato J. R., Cloutis E. A., Connolly Jr H. C., Hanna K. L. D., Emery J. P., Enos H. L., Fornasier S., Haberle C. W., Hanna R. D., Howell E. S., Kaplan H. H., and Keller L. P. 2019. Evidence for widespread hydrated minerals on asteroid (101955) Bennu. *Nature Astronomy* 3:332–340.

Houck J. R., Roellig T. L., van Cleve J., Forrest W. J., Herter T., Lawrence C. R., Matthews K., Reitsema H. J., Soifer B. T., Watson D. M., Weedman D., Huisjen M., Troeltzsch J., Barry D. J., Bernard-Salas J., Blacken C. E., Brandl B. R., Charmandaris V., Devost D., Gull G. E., Hall P., Henderson C. P., Higdon S. J. U., Pirger B. E., Schoenwald J., Sloan G. C., Uchida K. I., Appleton P. N., Armus L., Burgdorf M. J., Fajardo-Acosta S. B., Grillmair C. J., Ingalls J. G., Morris P. W., and Teplitz H. I. 2004. The infrared spectrograph (IRS) on the space telescope Spitzer. *Astrophysical Journal, The Supplement Series* 154:18–24.

Howard K. T., Benedix G. K., Bland P. A., and Cressey G. 2009. Modal mineralogy of CM2 chondrites by X-ray diffraction (PSD-XRD). Part 1: Total phyllosilicate abundance and the degree of aqueous alteration. *Geochimica et Cosmochimica Acta* 73:4576–4589.

Howard K. T., Benedix G. K., Bland P. A., and Cressey G. 2011. Modal mineralogy of CM chondrites by X-ray diffraction (PSD-XRD): Part 2. Degree, nature and settings of aqueous alteration. *Geochimica et Cosmochimica Acta* 75:2735–2751.

Howard K. T., Alexander C. M. O., Schrader D. L., and Dyl K. A. 2015. Classification of hydrous meteorites (CR, CM and C2 ungrouped) by phyllosilicate fraction: PSD-XRD modal mineralogy and planetesimal environments. *Geochimica et Cosmochimica Acta* 149:206–222.

Iwata T., Kitazato K., Abe M., Ohtake M., Arai T., Arai T., Hirata N., Hiroi T., Honda C., Imae N., Komatsu M., Matsunaga T., Matsuoka M., Matsuura S., Nakamura T., Nakato A., Nakauchi Y., Osawa T., Senshu H., Takagi Y., Tsumura K., Takato N., Watanabe S.-I., Barucci M. A., Palomba E., and Ozaki M. 2017. NIRS3: The near infrared spectrometer on Hayabusa2. *Space Science Reviews* 208:317–337.

King A. J., Schofield P. F., Howard K. T., and Russell S. S. 2015a. Modal mineralogy of CI and CI-like chondrites by X-ray diffraction. *Geochimica et Cosmochimica Acta* 165:148–160.

King A. J., Solomon J. R., Schofield P. F., and Russell S. S. 2015b. Characterising the CI and CI-like carbonaceous chondrites using thermogravimetric analysis and infrared spectroscopy. *Earth, Planets and Space* 67:198.

King A. J., Schofield P. F., and Russell S. S. 2017. Type 1 aqueous alteration in CM carbonaceous chondrites: Implications for the evolution of water-rich asteroids. *Meteoritics & Planetary Science* 52:1197–1215.

King A. J., Greenwood R. C, Gibson J. M., Schofield P. F., Franchi I. A., and Russell S. S. 2018. The oxygen isotopic composition of the most aqueously altered CM carbonaceous chondrites (abstract #2083). 49th Lunar and Planetary Science Conference. CD-ROM.

Kitazato K., Milliken R. E., Iwata T., Abe M., Ohtake M., Matsuura S., Arai T., Nakauchi Y., Nakamura T., Matsuoka M., Senshu H., Hirata N., Hiroi T., Pilorget C., Brunetto R., Poulet F., Riu L., Bibring J. P., Takir D., Domingue D. L., Vilas F., Barucci M. A., Perna D., Palomba E., Galiano A., Tsumura K., Osawa T., Komatsu M., Nakato A., Arai T., Takato N., Matsunaga T., Takagi Y., Matsumoto K., Kouyama T., Yokota Y., Tatsumi E., Sakatani N., Yamamoto Y., Okada T., Sugita S., Honda R., Morota T., Kameda S., Sawada H., Honda C., Yamada M., Suzuki H., Yoshioka K., Hayakawa M., Ogawa K., Cho Y., Shirai K., Shimaki Y., Hirata N., Yamaguchi A., Ogawa N., Terui F., Yamaguchi T., Takei Y., Saiki T., Nakazawa S., Tanaka S., Yoshikawa M., Watanabe S., and Tsuda Y. 2019. The surface composition of asteroid 162173 Ryugu from Hayabusa2 near-infrared spectroscopy. *Science* 364:272–275.

Lauretta D. S., Hua X., and Buseck P. R. 2000. Mineralogy of fine-grained rims in the ALH 81002 CM chondrite. *Geochimica et Cosmochimica Acta* 64:3263–3273.

Lauretta D. S., Balram-Knutson S. S., Beshore E., Boynton W. V., Drouet C. d'Aubigny, DellaGiustina D. N., Enos H. L., Golish D. R., Hergenrother C. W., Howell E. S., Bennett C. A., Morton E. T., Nolan M. C., Rizk B., Roper H. L., Bartels A. E., Bos B. J., Dworkin J. P., Highsmith D. E., Lorenz D. A., Lim L. F., Mink R., Moreau M. C., Nuth J. A., Reuter D. C., Simon A. A., Bierhaus E. B., Bryan B. H., Ballouz R., Barnouin O. S., Binzel R. P., Bottke W. F., Hamilton V. E., Walsh K. J., Chesley S. R., Christensen P. R., Clark B. E., Connolly H. C., Crombie M. K., Daly M. G., Emery J. P., McCoy T. J., McMahon J. W., Scheeres D. J., Nakamura-Messenger S., Righter K., and Sandford S. A. 2017. OSIRIS-REx: Sample return from asteroid (101955) Bennu. *Space Science Reviews* 212:925–984.

Licandro J., Hargrove K., Kelley M., Campins H., Ziffer J., Alí-Lagoa V., Fernández Y., and Rivkin A. 2012. 5–14 μm Spitzer spectra of Themis family asteroids. *Astronomy & Astrophysics* 537:A73.

Lim L. F., Barucci M. A., Campins H., Christensen P. R., Clark B., Delbo M., Emery J. P., Hamilton V. E., Lauretta D. S., and Licandro J. 2019. The global thermal infrared spectrum of (101955) Bennu in the context of Spitzer IRS asteroid spectra (abstract #1124). 50th Lunar and Planetary Science Conference. CD-ROM.

Lucey P. G., Honniball C. I., Gillis Davis J., Li S., and Hibbitts K. 2017. Water absorption at 6 microns: A new tool for remote measurements of lunar surface water abundance and variation. 48th Lunar and Planetary Science Conference. CD-ROM.

Marchis F., Enriquez J. E., Emery J. P., Mueller M., Baek M., Pollock J., Assafin M., Vieira Martins R., Berthier J., Vachier F., Cruikshank D. P., Lim L. F., Reichart D. E., Ivarsen K. M., Haislip J. B., and LaCluyze A. P. 2012. Multiple asteroid systems: Dimensions and thermal properties from Spitzer Space Telescope and ground-based observations. *Icarus* 221:1130–1161.

McAdam M. M., Sunshine J. M., Howard K. T., and Mccoy T. M. 2015. Aqueous alteration on asteroids: Linking the mineralogy and spectroscopy of CM and CI chondrites. *Icarus* 245:320–332.

McSween H. Y. Jr., Emery J. P., Rivkin A. S., Toplis M. J., Castillo-Rogez J. C., Prettyman T. H., Cristina De Sanctis M., Pieters C. M., Raymond C. A., and Russell C. T. 2017. Carbonaceous chondrites as analogs for the composition and alteration of Ceres. *Meteoritics & Planetary Science* 12:1–12.

Milliken R. E. and Rivkin A. S. 2009. Brucite and carbonate assemblages from altered olivine-rich materials on Ceres. *Nature Geoscience* 2:258–261.

Murakami H., Baba H., Barthel P., Clements D. L., Cohen M., Doi Y., Enya K., Figueredo E., Fujishiro N., Fujiwara H., Fujiwara M., Garcia-Lario P., Goto T., Hasegawa S., Hibi Y., Hirao T., Hiromoto N., Hong S. S., Imai K., Ishigaki M., Ishiguro M., Ishihara D., Ita Y., Jeong W.-S., Jeong K. S., Kaneda H., Kataza H., Kawada M., Kawai T., Kawamura A., Kessler M. F., Kester D., Kii T., Kim D. C., Kim W., Kobayashi H., Koo B. C., Kwon S. M., Lee H. M., Lorente R., Makiuti S., Matsuhara H., Matsumoto T., Matsuo H., Matsuura S., Mueller T. G., Murakami N., Nagata H., Nakagawa T., Naoi T., Narita M., Noda M., Oh S. H., Ohnishi A., Ohyama Y., Okada Y., Okuda H., Oliver S., Onaka T., Ootsubo T., Oyabu S., Pak S., Park Y. S., Pearson C. P., Rowan-Robinson M., Saito T., Sakon I., Salama A., Sato S., Savage R. S., Serjeant S., Shibai H., Shirahata M., Sohn J. J., Suzuki T., Takagi T., Takahashi H., Tanabe T., Takeuchi T. T., Takita S., Thomson M., Uemizu K., Ueno M., Usui F., Verdugo E., Wada T., Wang L., Watabe T., Watarai H., White G. J., Yamamura I., Yamauchi C., and Yasuda A. 2007. The infrared astronomical mission AKARI. *Publications of the Astronomical Society of Japan* 59:S369–S376.

Pommerol A., Schmitt B., Beck P., and Brissaud O. 2009. Water sorption on martian regolith analogs: Thermodynamics and near-infrared reflectance spectroscopy. *Icarus* 204:114–136.

Reuter D. C., Simon A. A., Hair J., Lunsford A., Manthripragada S., Bly V., Bos B., Brambora C., Caldwell E., Casto G., Dolch Z., Finneran P., Jennings D., Jhabvala M., Matson E., McLelland M., Roher W., Sullivan T., Weigle E., Wen Y., Wilson D., and Lauretta D. S. 2018. The OSIRIS-REx visible and infrared spectrometer (OVIRS): Spectral maps of the asteroid Bennu. *Space Science Reviews* 214:54.

Rivkin A. S. and Emery J. P. 2010. Detection of ice and organics on an asteroidal surface. *Nature* 464:1322–1323.

Rivkin A. S., Campins H., Emery J. P., Howell E. S., Licandro J., Takir D., and Vilas F. 2015. Astronomical observations of volatiles on asteroids. In *Asteroids IV*, edited by Michel P., DeMeo F. E., and Bottke W. F. Tucson, Arizona: The University of Arizona Press. pp. 65–87.

Russell C. T. and Raymond C. A. 2011. The Dawn mission to Vesta and Ceres. *Space Science Reviews* 163:3–23.

Ruzicka A., Grossman J. N., Bouvier A., Herd C. D. K., and Agee C. B. 2015. The Meteoritical Bulletin, No. 101. *Meteoritics & Planetary Science* 50:1661.

Salisbury J. W. 1993. Mid-infrared spectroscopy: Laboratory data. In *Remote geochemical analysis elemental and mineralogical composition*. Cambridge, UK: Cambridge University Press. pp. 79–98.

Salisbury J. W. and Walter L. S. 1989. Thermal infrared (2.5–13.5 μm) spectroscopic remote sensing of igneous rock types on particulate planetary surfaces. *Journal of Geophysical Research* 94:9192–9202.

Salisbury J. W., D'Aria D. M., and Jarosewich E. 1991. Midinfrared (2.5-23.5 μm) reflectance spectra of powdered stony meteorites. *Icarus* 92:280–297.

Tachibana S., Abe M., Arakawa M., Fujimoto M., Iijima Y., Ishiguro M., Kitazato K., Kobayashi N., Namiki N., Okada T., Okazaki R., Sawada H., Sugita S., Takano Y., Tanaka S., Watanabe S., Yoshikawa M., Kuninaka H.; The Hayabusa2 Team Project. 2014. Hayabusa2: Scientific importance of samples returned from C-type near-Earth asteroid (162173) 1999 JU3. *Geochemical Journal* 48:571–587.

Takir D., Emery J. P., Mcsween H. Y., Hibbitts C. A., Clark R. N., Pearson N., and Wang A. 2013. Nature and degree of aqueous alteration in CM and CI carbonaceous chondrites. *Meteoritics & Planetary Science* 48:1–20.

Takir D., Emery J. P., and Mcsween H. Y. 2015. Toward an understanding of phyllosilicate mineralogy in the outer main asteroid belt. *Icarus* 257:185–193.

Tholen D. J. 1984. Asteroid taxonomy from cluster analysis of photometry. PhD thesis, The University of Arizona, Tucson, Arizona.

Tomeoka K. and Buseck P. R. 1985. Indicators of aqueous alteration in CM carbonaceous chondrites: Microtextures

of a layered mineral containing Fe, S, O and Ni. *Geochimica et Cosmochimica Acta* 49:2149–2163.
Tomeoka K. and Buseck P. R. 1988. Matrix mineralogy of the Orgueil CI carbonaceous chondrite. *Geochimica et Cosmochimica Acta* 52:1627–1640.
Vernazza P., Marsset M., Beck P., Binzel R. P., Birlan M., Cloutis E. A., Demeo F. E., Dumas C., and Hiroi T. 2016. Compositional homogeneity of CM parent bodies. *The Astronomical Journal* 152:54–64.
Vernazza P., Castillo-Rogez J., Beck P., Emery J., Brunetto R., Delbo M., Marsset M., Marchis F., Groussin O., Zanda B., Lamy P., Jorda L., Mousis O., Delsanti A., Djouadi Z., Dionnet Z., Borondics F., and Carry B. 2017. Different origins or different evolutions? Decoding the spectral diversity among C-Type asteroids *The Astronomical Journal* 153:72–82.
Vilas F. 1994. A cheaper, faster, better way to detect water of hydration on solar system bodies. *Icarus1* 111:456–467.
Vilas F. and Gaffey M. J. 1989. Phyllosilicate absorption features in main-belt and outer-belt asteroid reflectance spectra. *Science* 246:790–792.
Vilas F., Jarvis K. S., and Gaffey M. J. 1994. Iron alteration minerals in the visible and near-infrared spectra of low-albedo asteroids. *Icarus* 109:274–283.
Zolensky M. E., Bourcier W. L., and Gooding J. L. 1989. Aqueous alteration on the hydrous asteroids—Results of EQ3/6 computer simulations. *Icarus* 78:411–425.
Zolensky M. E., Mittlefehldt D. W., Lipschutz M. E., Wang M.-S., Clayton R. N., Mayeda T. K., Grady M. M., Pillinger C., and Barber D. 1997. CM chondrites exhibit the complete petrologic range from type 2 to 1. *Geochimica et Cosmochimica Acta* 61:5099–5115.

SUPPORTING INFORMATION

Additional supporting information may be found in the online version of this article.

Appendix S1: Thermogravimetric analysis of the highly hydrated CM and CI chondrites.

Fig. S1. Typical mass loss and DTG curves for CM1/2 and CM1 chondrites. The CM1/2 and CM1 chondrites show significant mass loss between 400 and 770 °C due to dehydration of abundant serpentine phyllosilicate minerals. Mass loss under 200 °C is attributed to adsorbed terrestrial water. GRO 95645 and MIL 07689, the most weathered samples investigated, show dehydration of a phase at ~225 °C, which is within the region where Fe-(oxy)hydroxides dehydrate and is likely a terrestrial weathering product.

Table S1. Mass loss (wt%) for the CM2, CM1/2, CM1, and CI1 chondrites as a function of different temperature ranges. Most mass loss occurs in the 400–770 °C range, which is consistent with the dehydration and dehydroxylation of phyllosilicate phases.

Data S1. The spectral data for the CM2, CM1/2, CM1, and CI1 chondrites, from 1.70 – 77 μm.